Discovery of a Novel cGAMP Exporter that Regulates Innate Antiviral Immunity

Joanna Maltbaek

A dissertation

submitted in partial fulfillment of the

requirements for the degree of

Doctor of Philosophy

University of Washington

2022

Reading Committee:

Daniel B. Stetson, Chair

Jessica Hamerman

Ram Savan

Program Authorized to Offer Degree:
Department of Immunology

University of Washington

Abstract

Discovery of a Novel cGAMP Exporter that Regulates Innate Antiviral Immunity

Joanna Maltbaek

Chair of the Supervisory Committee:

Daniel B. Stetson

Department of Immunology

The DNA sensor cyclic GMP-AMP synthase (cGAS) is important for antiviral and anti-tumor immunity. cGAS generates cyclic GMP-AMP (cGAMP), a diffusible cyclic dinucleotide that activates the antiviral response through the adapter protein Stimulator of Interferon Genes (STING). cGAMP cannot passively cross cell membranes, but recent advances have established a role for extracellular cGAMP as an “immunotransmitter” that can be imported into cells. The mechanism by which cGAMP exits cells remains unknown. Here, we identify ABCC1/MRP1 as an ATP-dependent cGAMP exporter. We show that ABCC1 overexpression enhances cGAMP export and limits STING signaling, and that loss of ABCC1 reduces cGAMP export and potentiates STING signaling. We demonstrate that ABCC1 deficiency exacerbates cGAS-dependent autoimmunity in the *Trex1*$^{-/-}$ mouse model of Aicardi-Goutières syndrome. These studies identify ABCC1-mediated cGAMP export as a key regulatory mechanism that limits cell intrinsic activation of STING and ameliorates STING-dependent autoimmune disease.

Table of Contents

Acknowledgements:

I am forever indebted to my thesis advisor, Dan Stetson. Thank you, Dan, for your reckless optimism and love for teaching. I was new to the field of innate immunity, and never once did you make me feel as though I didn't belong or that I couldn't succeed. My love for the project and confidence as a scientist grew as a direct result of your unwavering support and enthusiasm. I am so grateful that I got to train in your lab.

To all the members of the Stetson Lab, thank you for making my time in graduate school some of the best years of my life. I knew going to graduate school would be hard, but I never realized it would also be insanely fun. To Steph, thank you for keeping the lab running like a well-oiled machine. To Hannah, thank you for answering my endless questions and providing creative ideas for experiments. To Katie and Meegan, thank you being such great examples of hard work and perseverance to finish the PhD. And to Emily, thank you for being my lab BFF!

I'd also like to acknowledge the UW Department of Immunology as a whole: to all the students, postdocs, and staff, thank you for making this such a phenomenal place to work. Thank you especially to my thesis committee members: Marion Pepper, Jessica Hamerman, Ram Savan, and Joshua Woodward, for all the great ideas and insightful discussions throughout the years.

I wouldn't be pursuing this degree if it weren't for the support of my first mentor in science, Dr. Fenna Sillé. Thank you, Fenna, for mentoring me throughout your postdoc and introducing me to the wonders of the immune system when I was a young undergrad with no real lab experience. Most importantly, thank you for your patience! Thank you to Dr. Martyn Smith from UC Berkeley School of Public Health for taking me into the lab during undergrad and to Dr. Ron DeMatteo of Memorial Sloan Kettering Cancer Center for giving me a home for two years as a research technician while I pondered the next steps of my career.

Finally, to my friends: thank you for the humor and for all the support through 22 years of schooling. To my fiancé, Ty Crowl: I couldn't have finished this degree without your love and care to uplift me. To my family, especially to my parents, Peter and Tina Maltbaek: thank you for cheering me on and giving me the tools to succeed. Everything good in my life is the product of your hard work and benevolence. I love you beyond measure.

For my grandparents:

Kathleen Maltbæk (1930 -)

Dr. Jørgen Maltbæk (1923 - 2021)

Hermione Pearson (1926 - 2008)

John Pearson (1922 - 2010)

Chapter 1: Introduction

Innate Immunity during Viral Infection

The ability to detect self from nonself is an essential requirement of the immune response against pathogens. Pattern recognition, a theory first postulated by Charles Janeway Jr. in 1989, states that innate immune recognition relies on nonclonal, germline encoded receptors that detect evolutionary conserved features of microorganisms[1]. This contrasts with adaptive immunity, where somatic recombination of lymphocyte antigen receptor gene fragments creates an endlessly diverse array of pathogen-specific receptors. While the adaptive arm of the immune system results in specific, long-lasting protection against pathogens, it initially relies on priming signals from the innate immune system and then takes time to generate and become finely tuned. As such, the innate immune system is important for the initial early warning system of pathogen detection. It employs so-called pattern recognition receptors (PRRs) to recognize common elements of pathogens. For example, lipopolysaccharides and peptidoglycans of bacterial cell walls as well as unique sugars found in fungal cell walls are evolutionarily conserved for these microorganisms and not found in vertebrates. Thus, these are straightforward targets for PRRs. Viruses, however, represent an interesting challenge within this framework because they recruit host proteins for their replication, and every component of new virions is derived from the infected host. Most host recognition of viruses involves sensors that detect foreign nucleic acids, as all viruses have a genome composed of either RNA or DNA. However, host RNA and DNA are abundant inside cells, which underscores the importance of nucleic acid sensors properly discriminating between self and nonself to avoid inappropriate immune activation.

In prokaryotes, restriction enzymes represent an example of a mechanism of self/nonself discrimination. Restriction enzymes are DNA endonucleases that cleave specific DNA sequences in bacteriophages that are either absent in host nucleic acids or shrouded by host modifications[2]. Another example can be found with early eukaryote argonaute proteins and RNA

interference, which recognize and antagonize foreign RNA[3]. Importantly, however, these mechanisms are sequence-specific and thus self-limiting in nature. Vertebrate nucleic acid sensors, in contrast, can recognize more broadly shared characteristics of viruses that are distinct from mammalian cellular components, such as unique nucleic acid structures or subcellular localizations that are unusual for host nucleic acids.

Upon recognition of viral nucleic acids, PRRs induce the production of the potent antiviral cytokine interferon (IFN). Type I IFN, specifically IFNβ, is the first of over one dozen IFN genes encoded by vertebrates[4] that is produced downstream of PRR activation. Type I IFN acts in both an autocrine and paracrine manner to signal through the heterodimeric type I IFN receptor (IFNAR). IFNAR is expressed by most cell types and can initiate the production of many hundreds of IFN-stimulated genes (ISGs). ISGs have varying functions, from direct viral antagonism to the recruitment of immune cells through chemokine production. The expression of ISGs is responsible for the antiviral reprogramming of the infected tissue that is ultimately required for productive antiviral immunity.

Types of Nucleic Acid Sensors

In mammals, there are two categories of nucleic acid sensors that can be differentiated by the compartment in which they recognize their cognate ligands. The first category is comprised of Toll-like receptors (TLRs), some of which recognize exogenous nucleic acids. TLR3 can recognize double-stranded RNA (dsRNA), TLR7/8 can recognize single-stranded RNA (ssRNA), and TLR9 can recognize double-stranded DNA (dsDNA)[5]. These TLRs survey the extracellular environment for foreign nucleic acids, both by cell surface expression and endosomal localization. As such, their expression is primarily restricted to phagocytic immune cells, which allows for increased potential in encountering their respective ligands. TLRs 3 and 4 signal through the adaptor protein TIR-domain-containing adapter-inducing interferon-β (TRIF) to activate the kinase TANK binding kinase 1 (TBK1) and subsequently the transcription factor Interferon Regulatory Factor 3 (IRF3), which will initiate the production of Type I IFN[6]. TLRs 7,

8, and 9 signal through the adaptor protein Myeloid Differentiation primary response 88 (MyD88), which activates the kinase Inhibitor of nuclear factor Kappa-B Kinase subunit alpha (IKKα), and subsequently activates the transcription factor Interferon Regulatory Factor 7 (IRF7) for Type I IFN production[7].

The second category of nucleic acid sensors survey the intracellular environment, in both the cytosol and the nucleus, for the presence of viral nucleic acids. Unlike the limited expression pattern of the TLRs, these sensors are more widely expressed and found in nearly every vertebrate cell type. Viral RNA recognition depends on the cytosolic sensors Melanoma Differentiation Associated protein 5 (MDA5) and the Retinoic Acid inducible gene I (RIG-I), which are activated by long dsRNA or 5' triphosphate RNA, respectively[8]. Importantly, the structural features of these RNA ligands are not commonly found in host RNA ligands in the cytosol: 5' triphosphate ends are typically removed from host mRNAs prior to their transport to the cytosol, while long dsRNA structures are primarily intronic and therefore removed via splicing before cytosolic entry. In contrast, the primary DNA sensor cyclic GMP-AMP Synthase (cGAS) binds to the sugar phosphate backbone of dsDNA, regardless of its sequence, meaning cGAS can become activated upon binding to host as well as viral DNA[9]. Interestingly, while cGAS can be found in the cytosol, it is primarily a nuclear protein[10] and is tightly tethered to chromatin in an inactive state[11-15]. How cGAS becomes untethered and whether cGAS physically binds to viral-derived dsDNA and/or host-derived dsDNA during virus infection remains to be determined.

Both the RNA and DNA sensors signal through unique adaptor proteins. cGAS activation catalyzes the synthesis of 2',3'-cyclic GMP-AMP (cGAMP)[16, 17], a diffusible second messenger cyclic dinucleotide (CDN) that binds to the adaptor STimulator of Interferon Genes (STING) to induce the phosphorylation of the kinase TBK1[9, 18]. The RNA sensors signal through the adaptor Mitochondrial AntiViral Signaling protein (MAVS)[19] which similarly recruits and activates TBK1.

In both pathways, TBK1 activation results in the phosphorylation of the transcription factor IRF3, which will dimerize, translocate to the nucleus, and initiate the production of Type I IFN.

Negative Regulation of Nucleic Acid Sensing Pathways

Type I IFN, while being potently antiviral, can also be pathogenic in nature if it is aberrantly produced[20]. Thus, the production of Type I IFN must be tightly regulated to prevent the development of autoimmune diseases known as “interferonopathies,” which can be classified by a Type I IFN signature in peripheral blood cells that drives rampant tissue damage[21]. The nucleic acid sensors have perhaps the highest potential amongst PRRs for encountering endogenous ligands. To accommodate for this, cells express numerous accessory enzymes that aid in self/nonself discrimination. There are three known enzymes that limit the activation of cGAS by endogenous DNA: Three prime Repair Exonuclease 1 (TREX1), RNaseH2, and SAM domain and HD domain-containing protein 1 (SAMHD1). These enzymes act to either cleave or degrade their target DNA or RNA-DNA hybrid ligands, thus preventing inappropriate cGAS activation[22-24]. RNA sensors similarly employ negative regulators that act to promote RNA degradation at the steady state, including Ski2 Like RNA Helicase (SKIV2L) and Adenosine Deaminase Acting on dsRNA (ADAR1)[25, 26]. Mutations in both nucleic acid sensors and their respective negative regulators can underlie Aicardi-Goutières Syndrome (AGS), a rare and severe disease that resembles congenital viral infection and leads to severe intellectual and motor dysfunction[21]. Therefore, understanding and characterizing the various mechanisms that negatively regulate nucleic acid sensing is paramount to identifying treatment targets for interferonopathies.

cGAMP in Time and Space

The focus of this thesis is an exploration of how cGAMP is regulated and degraded by the cell. Much attention has been given to how the signaling proteins and kinases implicated in cGAS-STING signaling are regulated and degraded, but the precise mechanism of cGAMP degradation remains comparatively unexplored. The formation of cGAMP by cGAS has its roots

in ancient nucleotidyltransferases that regulate signaling and metabolism in prokaryotes[27, 28]. Like all RNA nucleotide-based second messengers that exist across all kingdoms of life[29], cGAMP is unable to passively enter or exit cells because of its two negatively charged phosphate groups that prevent movement across hydrophobic phospholipid bilayers that make up cellular membranes. Thus, studies on the cGAS-STING DNA sensing pathway have focused on the basic cGAMP signaling dynamics that occur intracellularly. However, recent advances have challenged the notion that cGAMP is solely an intracellular signaling molecule. In 2014, the first (and so far, only) metazoan phosphodiesterase capable of hydrolyzing cGAMP was identified: EctoNucleotide Pyrophosphatase/Phosphodiesterase 1 (ENPP1)[30], which converts cGAMP into GMP and AMP. The identification of a cGAMP phosphodiesterase should have been a welcome insight, considering that all other cyclic nucleotides are regulated by phosphodiesterases (cyclic AMP, cyclic GMP, etc)[29]. However, this finding was largely ignored by the field because of a topological problem: ENPP1 is a transmembrane protein oriented such that its catalytic domain is in the extracellular space, and thus would not have access to intracellular cGAMP. It was previously shown that cGAMP can signal beyond its cell of origin via movement through gap junctions[31] and packaging into enveloped viral particles[32, 33]; however, in these scenarios, cGAMP is never exposed to the extracellular space. The first critical insights into the existence of extracellular cGAMP came from a recent study that demonstrated that cGAMP is released by tumor cells and sensed by host myeloid cells to mediate anti-tumor immunity[34]. It was also later demonstrated that this extracellular pool of cGAMP is subject to potent regulation by ENPP1-mediated degradation[35]. Moreover, in the last few years, numerous studies have shown that extracellular cGAMP can be taken up by various importer channels and activate STING signaling in distant cells[36-41].

Whereas extracellular cGAMP and its import into cells have now been described, one fundamental question remains: how does cGAMP exit the cells that produce it? This is an important question because a deeper understanding of cGAMP export mechanisms will fill

critical gaps in our knowledge of cGAMP dynamics and enable mechanistic studies into the role of extracellular cGAMP in autoimmune disease and tumor immunotherapy. In this thesis, we identify a putative cGAMP exporter and demonstrate its importance for negatively regulating antiviral responses and controlling cGAS-dependent autoimmunity.

Chapter 1 Figures

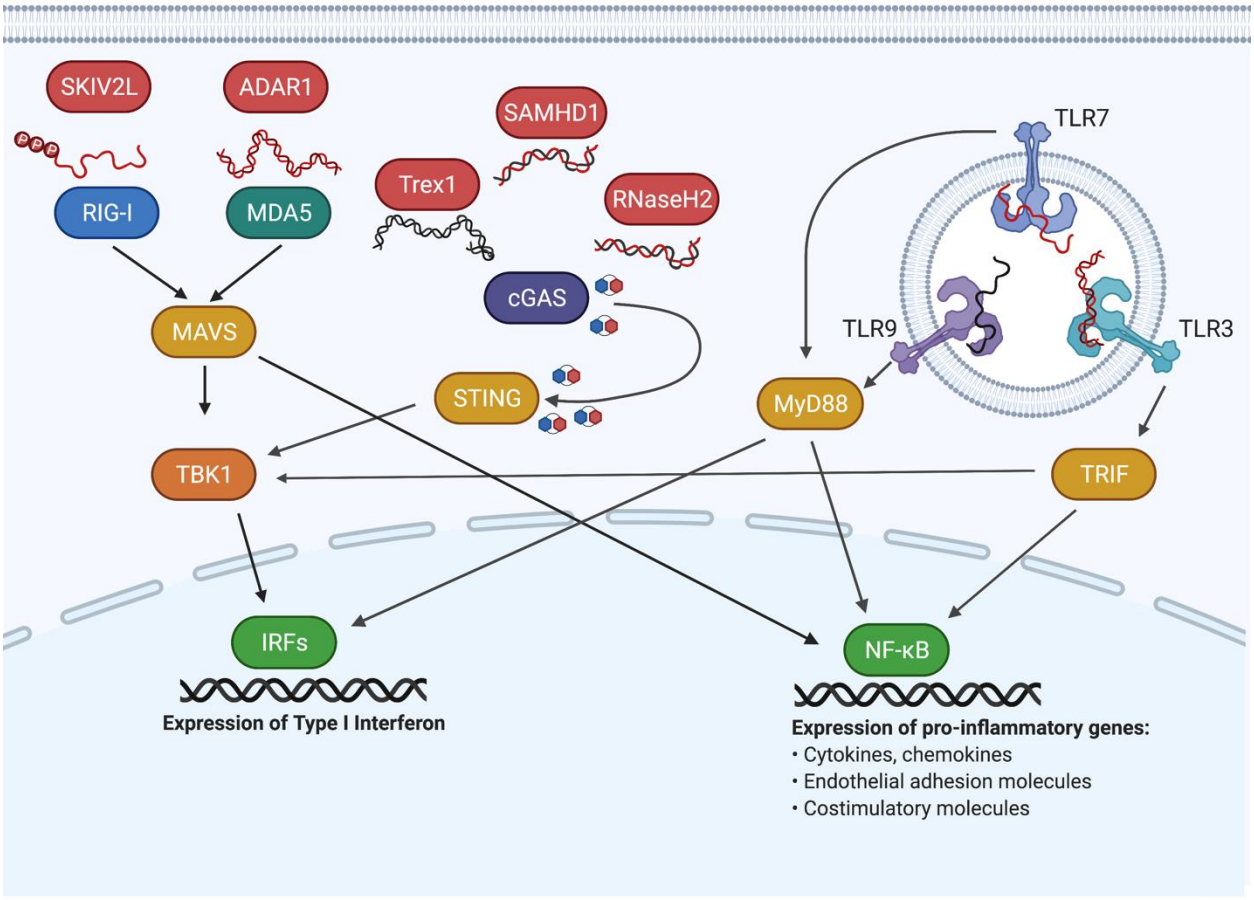

Figure 1.1: Summary of known metazoan nucleic acid sensing pathways, depicted with negative regulators, adaptor proteins, and transcriptional outcomes.

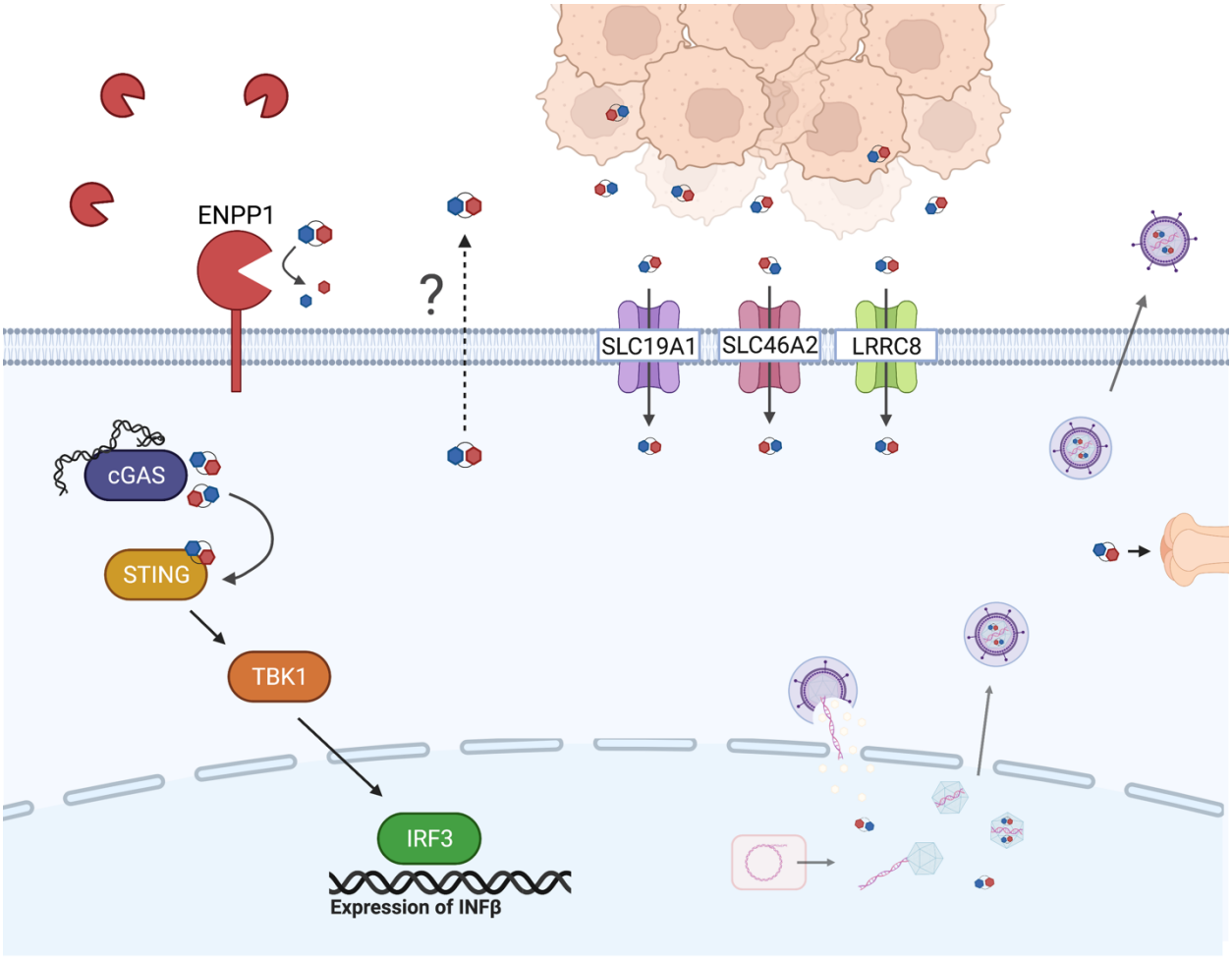

Figure 1.2: Background on the current state of cGAMP transport. cGAMP can be transported to neighboring cells via gap junctions or found packaged in new virions and transported to new cells via viral infection. Tumor cells are a source of extracellular cGAMP. Extracellular cGAMP can be taken up by cGAMP importers, depicted here at the cell membrane. No precise mechanism for cGAMP export has been described.

Sections of text in the remaining chapters have been modified slightly from the following manuscript:

Maltbaek JH, Snyder JM, Stetson DB. ABCC1 exports cGAMP and modulates cGAS-dependent immunity. *BioRxiv 2021*.

Chapter 2: cGAMP export occurs in primary cells and is pharmacologically targetable

Introduction

The only known mechanism for cGAMP degradation is via the extracellular enzyme ENPP1[30]. Tumor cells can be a source of extracellular cGAMP[34, 35], but it is unclear if live, primary cells can export cGAMP or if it is simply released passively during cell death. We considered the mechanisms by which cGAMP could be exported from live cells, if inflammatory cell death was not the main source of extracellular cGAMP. Previous studies have shown that cGAMP can be enclosed in extracellular vesicles[32, 33], and a more recent study demonstrated that cGAMP can be exported as a soluble factor[35]. We therefore focused on transmembrane channels and transporters as potential cGAMP exporters. There are two broad classes of such proteins: 1) channels that passively export substrates based on electrochemical gradients, and 2) transporters that use the energy of ATP hydrolysis to move substrates across membranes, sometimes against a concentration gradient. We focused on active transport mechanisms that are accomplished by the ATP-binding cassette (ABC) family of transmembrane proteins[42], guided by the prior identification of bacterial ATP-dependent export channels that mediate efflux of cyclic dinucleotides[27]. Human ABC transporters are named because of a shared intracellular domain that binds ATP and translates the energy of ATP hydrolysis into conformational changes that move substrates from the cytosol to extracellular space or into membrane-bound intracellular compartments. The human genome encodes 49 ABC transporters that move a broad spectrum of small molecules with diverse masses and chemical properties[43]. Many ABC transporters have been scrutinized because of their ability to export chemotherapeutic drugs[44, 45], which has resulted in the development of numerous pharmacological inhibitors of entire families of ABC transporters. We therefore assessed the ability of these various inhibitors to

block cGAMP export. Moreover, to enable screening of candidate transporters, we designed a lentiCRISPR screen in primary mouse bone marrow macrophages (BMM) to disrupt genes of interest for the assessment of loss of cGAMP export during DNA stimulation.

Results

cGAMP is exported from live cells

Intracellular DNA detection activates both the cGAS-cGAMP-STING pathway to trigger IFN-mediated antiviral responses and the AIM2 inflammasome to activate rapid, inflammatory cell death known as pyroptosis[46, 47]. This AIM2-dependent cell death pathway is particularly potent in myeloid cells, although it can function in non-myeloid cell types[48]. To study cGAMP dynamics in the absence of the AIM2 inflammasome, we prepared primary bone marrow derived macrophages (BMMs) from mice lacking all 13 mouse AIM2-like receptors (ALRs)[49]. As previously reported, we found that DNA-activated rapid cell death was almost completely abolished in *ALR*$^{-/-}$ BMMs (Fig. 2.1A). We then measured intracellular and extracellular concentrations of cGAMP 8 hours after transfection with calf thymus (CT) DNA using a sensitive cGAMP ELISA[10, 50]. We normalized the input volumes of cell extracts and extracellular media to allow direct comparison of absolute cGAMP amounts between these two compartments. We found that *ALR*$^{-/-}$ BMMs produced significantly more total cGAMP than WT control BMMs, consistent with the enhanced IFN responses in AIM2- and ALR-deficient mice (Fig. 2.1B)[46, 49]. However, we recovered the majority of this cGAMP from the extracellular media, not from inside the cells (Fig. 2.1B). Finally, *ALR*$^{-/-}$*Sting*$^{-/-}$ double knockout (DKO) BMMs exported similar amounts of cGAMP compared to *ALR*$^{-/-}$ BMMs (Fig. 2.1B), demonstrating that STING signaling was not required for cGAMP export.

We next tested primary murine embryonic fibroblasts (MEFs), which do not undergo ALR-dependent pyroptosis in response to DNA detection (Fig. 2.1C)[49]. We found that MEFs exported significant amounts of cGAMP in the absence of cell death (Fig. 2.1D), but not as much as BMMs in relative extracellular versus intracellular cGAMP amounts (Fig. 2.1B). We extended these findings to immortalized human foreskin fibroblasts (HFF) and human tumor cell lines, including A549 lung adenocarcinoma cells[51], HeLa cervical carcinoma[52], and Me275 melanoma cells[53]. We first verified that none of these cells expressed detectable levels of

Enpp1 mRNA or ENPP1 protein (Fig. 2.2A, 2.2B). We found that the amount of extracellular cGAMP was low or nearly absent in HFF, HeLa, and Me275 cells, even though these cells all produced detectable intracellular cGAMP in response to DNA transfection (Fig. 2.2C). A549 cells were the only human cell type tested that exported cGAMP at levels comparable to mouse BMMs (Fig. 2.1E). Finally, we filtered supernatants from each cell type through 10 kDa filter, which should remove all exosomes. We found that the amount of extracellular cGAMP before and after filtration was unchanged, meaning that extracellular cGAMP was not contained within exosomes and was likely soluble (Fig. 2.2D). Thus, we have found that live cells export cGAMP, and we have identified a nearly 60-fold range of export "efficiency" among diverse mouse and human cell types (Fig. 2.1E).

Identification of a drug that blocks cGAMP export

We used three inhibitors of distinct classes of ABC transporters and measured their effect on cGAMP export from ALR KO BMMs: verapamil, which inhibits the ABCB1 transporter[54]; KO-143, which blocks the ABCG2 transporter[55]; and MK-571, a drug developed as an ABCC1 inhibitor[56]. We found that verapamil did not influence cGAMP export, but pretreatment with MK-571 resulted in a significant, dose-dependent increase in intracellular cGAMP after DNA transfection (Fig. 2.3A), consistent with blockade of cGAMP export. The highest dose of KO-143 also significantly increased intracellular cGAMP, but it was previously reported that KO-143 has an inhibitory effect on the transport activity of both ABCB1 and ABCC1 at this concentration[57]. Thus, we focused on the dose-dependent blockade of cGAMP export by MK-571. MK-571 pretreatment not only resulted in enhanced retention but also reduced export of cGAMP from BMMs (Fig. 2.3B). We extended these findings to human cells including A549 (Fig. 2.3C) and HFF (Fig. 2.3D). As with mouse cells, pre-treatment with MK-571 resulted in enhanced retention of cGAMP after DNA transfection in each human cell type. Furthermore, A549 cells treated with MK-571 had reduced cGAMP export (Fig. 2.3C), though

extracellular cGAMP levels were low in HFF (Fig. 2.3D). These data demonstrate that MK-571 potently blocks cGAMP export in both mouse and human cells.

ABCC1 is a cGAMP exporter

MK-571 inhibits ABCC1, also known as multidrug resistance protein 1 (MRP1)[58], which has been demonstrated to mediate the export of cysteinyl LTC4, the conjugated estrogen $E_2$17βG, oxidized glutathione (GSH)[59], and sphingosine-1-phosphate[60]. ABCC1 is a member of a family that includes several related transporters, and it is now known that MK-571 blocks other members of the ABCC/MRP family, including ABCC2/MRP2, ABCC4/MRP4, and ABCC5/MRP5[61, 62]. We developed quantitative RT-PCR assays to measure the expression of each member of the ABCC/MRP family. Moreover, to enable screening of potential candidate transporters using lentiCRISPR in primary BMMs, we crossed our ALR KO mice with mice that constitutively express Cas9[63]. We found that ALR KO-Cas9 BMMs expressed detectable mRNA transcripts for five of the eight ABCC family members (Fig. 2.4A). We designed guide RNAs (gRNAs) to target these five expressed ABCC channels, cloned them into a lentiCRISPR vector, prepared lentivirus particles, and transduced primary BMMs followed by selection in puromycin[10, 49, 50, 64]. As a control for transduction and for off-target effects, we included a gRNA targeting *Abcc6*, which was not expressed in BMMs (Fig. 2.4A). After selection, we observed significant but incomplete disruption of the target genes using TIDE analysis (Tracking of Indels by Decomposition)[65] (Fig. 2.4B). We found that disruption of *Abcc1*, but not any of the other expressed *Abcc* genes, resulted in a significant decrease in the percent of extracellular cGAMP recovered following DNA transfection (Fig. 2.4C, Fig. 2.5A). We repeated this experiment, including an additional M1 non-targeting control gRNA, together with a second gRNA targeting a distinct site in the *Abcc1* gene. Both *Abcc1* gRNAs depleted ABCC1 protein levels (Fig. 2.4D) and decreased extracellular cGAMP (Fig. 2.4E, Fig. 2.5B). To assess whether *Abcc1* is responsible for all cGAMP export in BMMs, we crossed ABCC1-deficient mice to our ALR KO mice. Heterozygous *Abcc1*$^{+/-}$ALR$^{-/-}$ BMMs had reduced ABCC1 protein levels, whereas

homozygous *Abcc1*$^{-/-}$*ALR*$^{-/-}$ BMMs lacked ABCC1 protein expression (Fig. 2.4F). We found a significant reduction in extracellular cGAMP after DNA stimulation in both *Abcc1*$^{+/-}$ and *Abcc1*$^{-/-}$ BMMs compared to controls (Fig. 2.4G, Fig. 2.5C). Pretreatment with MK-571 further reduced cGAMP export (Fig. 2.4G, Fig. 2.5C). These data demonstrate that ABCC1 is responsible for a significant fraction of cGAMP export in BMMs, and that these cells have additional transport mechanism(s) that are sensitive to MK-571.

Next, we tested whether disruption of *ABCC1* reduces cGAMP export in human cells. We designed two distinct gRNAs to target human *ABCC1* with lentiCRISPR as described above. We first tested these gRNAs in A549s and found that they depleted ABCC1 protein (Fig. 2.5H). We assessed functional loss of ABCC1 transport activity following targeting using Fluo-3, a calcium-binding fluorescent compound that is a known substrate of ABCC1-dependent export[66, 67]. We used measurement of Fluo-3 fluorescence as a proxy for ABCC1 activity: cells with high ABCC1 activity were dimmer than cells with low ABCC1 activity (Fig. 2.5D). Flow cytometry analysis showed that *ABCC1* targeted A549 cells had a significant increase in Fluo-3 mean fluorescence intensity (MFI) compared to H1 control targeted cells, demonstrating that these gRNAs reduce ABCC1 transport activity (Fig. 2.5E, 2.5F). *ABCC1* targeted A549 cells had a significant decrease in percentage of extracellular cGAMP compared to control H1 targeted cells (Fig. 2.4I, Fig. 2.5G). We then targeted *ABCC1* in HFFs (Fig. 2.4J), and we found a significant decrease in the percent of extracellular cGAMP in the *ABCC1*-targeted cells compared to H1 control targeted cells (Fig. 2.4K, Fig. 2.5H). Taken together, these data demonstrate that disruption of human *ABCC1* reduces cGAMP export. Moreover, and like *Abcc1*$^{-/-}$ mouse cells (Fig. 2.4G), additional cGAMP export mechanism(s) exist in human cells that are sensitive to MK-571 (Figure 2.3C, 2.3D).

Discussion

While inflammatory pyroptotic cell death does contribute to extracellular cGAMP (Fig. 2.1B), we demonstrate that live, intact cells contribute significantly more to the pool of extracellular cGAMP following cGAS activation. We initially hypothesized that this export mechanism might be STING dependent: cGAMP exporter could be coupled to activation of STING itself or else interferon-inducible. However, given that STING-knockout cells still export cGAMP, we conclude that the cGAMP exporter must be active independent of STING. This pool of extracellular cGAMP is soluble and we did not find that exosomes contained significant extracellular cGAMP. We also identified highly variable cGAMP export efficiencies across multiple human cancer cell lines. Since ENPP1 can potently degrade the pool of extracellular cGAMP, we verified that the cells used in our study don't express ENPP1.

In our drug screen, while we identified MK-571 as the most prominent inhibitor of cGAMP export, we noted that KO-143 also had an inhibitory effect against export, albeit at high concentrations. The ABC transporters do share a variety of overlapping substrate specificities, so we retain that it is possible that the main target of KO-143, ABCG2, could also be a (less active) exporter of cGAMP. Additionally, genetic disruption of *ABCC1* reduced but did not completely ablate cGAMP export *in vitro*, further suggesting that alternative cGAMP export mechanisms exist. This is perhaps unsurprising considering that multiple cGAMP importer channels have been identified to date[36-41]. It was recently proposed that the LRRC8-containing volume regulated anion channel (VRAC) might serve as a "passive" cGAMP exporter, but these studies clearly demonstrated that LRRC8 can only export cGAMP under artificial hypotonic conditions that activate the channel through cell swelling[38, 39]. While our CRISPR screen did not implicate other ABCC/MRP family members in cGAMP export, our finding that MK-571 further inhibits cGAMP export in *Abcc1*$^{-/-}$ BMMs and the fact that other nucleotide derivates such as cyclic AMP and cyclic GMP can be moved by ABCC family proteins[68-70] suggest that cGAMP might be a substrate of multiple ABC transporters. To identify additional cGAMP exporters, our

ALR-deficient, Cas9-expressing mice remain a valuable tool for CRISPR-based screens in primary cells. Regardless of the potential for multiple cGAMP export mechanisms, based on these data, we emphasize that ABCC1 plays a nonredundant role in cGAMP export *in vitro*.

Finally, there have been numerous recent advances in our understanding of the ancient evolutionary origins of the cGAS-STING pathway. These include the discoveries of diverse cGAS orthologs, the generation of 2'-5'-linked oligonucleotides, and the functional conservation of STING in prokaryotic antiviral immunity[71-75]. Our identification of ABCC1 as a putative cGAMP exporter in mammals raises interesting comparisons to the regulation of intracellular CDN concentrations in prokaryotes. The ABC transporter superfamily exists not only in eukaryotes but also prokaryotes and archaea[76], and the regulation of intracellular CDN concentrations through energy-dependent efflux is documented in bacteria[27]. We postulate that cGAMP export by ABCC1 fits into this framework in which the central regulatory components involved in mammalian cGAS-STING signaling all evolved from ancient mechanisms of defense against bacteriophages. A detailed evolutionary analysis is called for to explore this intriguing possibility. The possibility that ABCC1 exports other CDNs, such as those of microbial origin, also remains to be determined.

Chapter 2 Figures

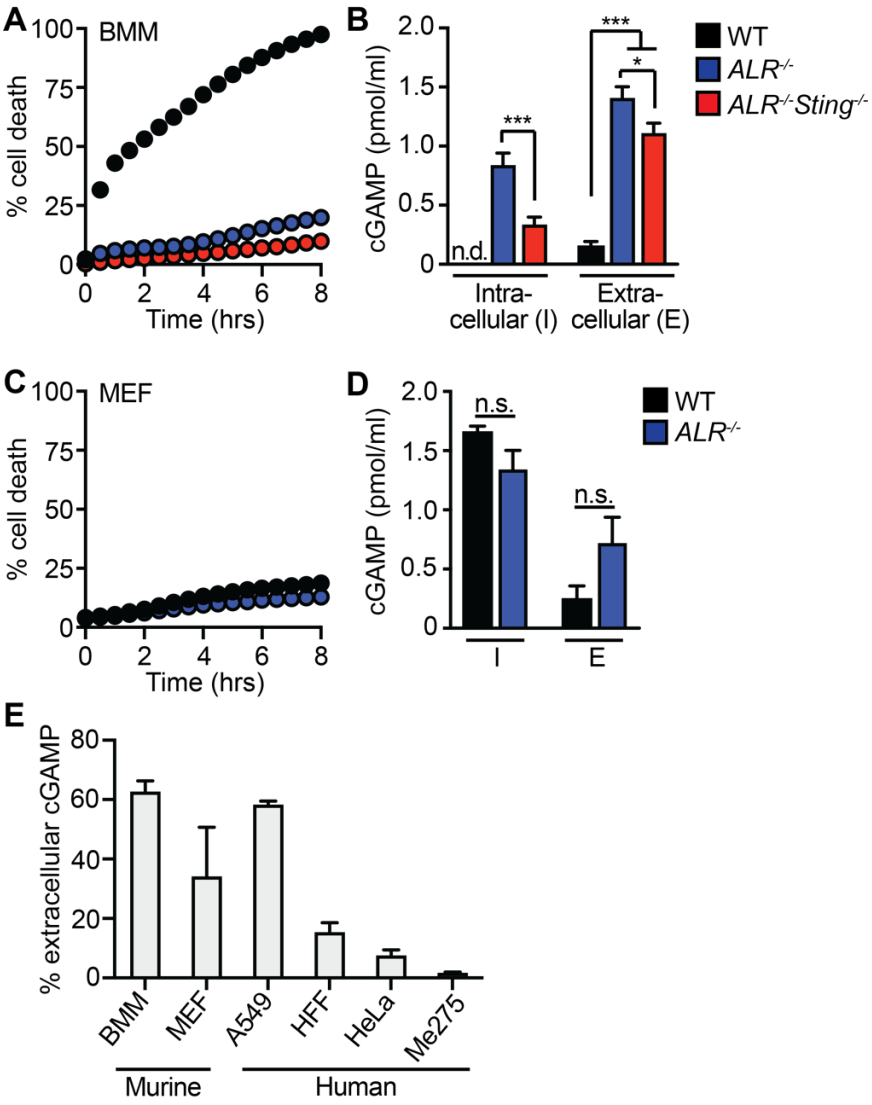

Figure 2.1: (A) Cell death of BMMs from WT, *ALR*$^{-/-}$, *ALR*$^{-/-}$*Sting*$^{-/-}$ mice transfected with calf thymus DNA (CT DNA) quantified using an IncuCyte imaging system. (B) cGAMP quantification using ELISA from cell lysates and supernatants in (A) 8 hours after transfection. (C) Cell death of MEFs from WT or *ALR*$^{-/-}$ mice transfected with CT-DNA quantified using an IncuCyte imaging system. (D) cGAMP quantification using ELISA from cell lysates and supernatants in (C) 8 hours after transfection. (E) Percent extracellular cGAMP of indicated cell types 8 hours after CT DNA transfection. cGAMP ELISA was used to determine relative extracellular and intracellular concentrations before calculating the percent extracellular. Statistical analysis was performed using a two-way ANOVA comparing cell lines within I or E compartments (B, D). Error bars represent mean ± SD of three biological replicates per group. *p<0.05, ***p<0.001. All data shown are derived from a single representative experiment. Comparative results were obtained across 3 independent experiments.

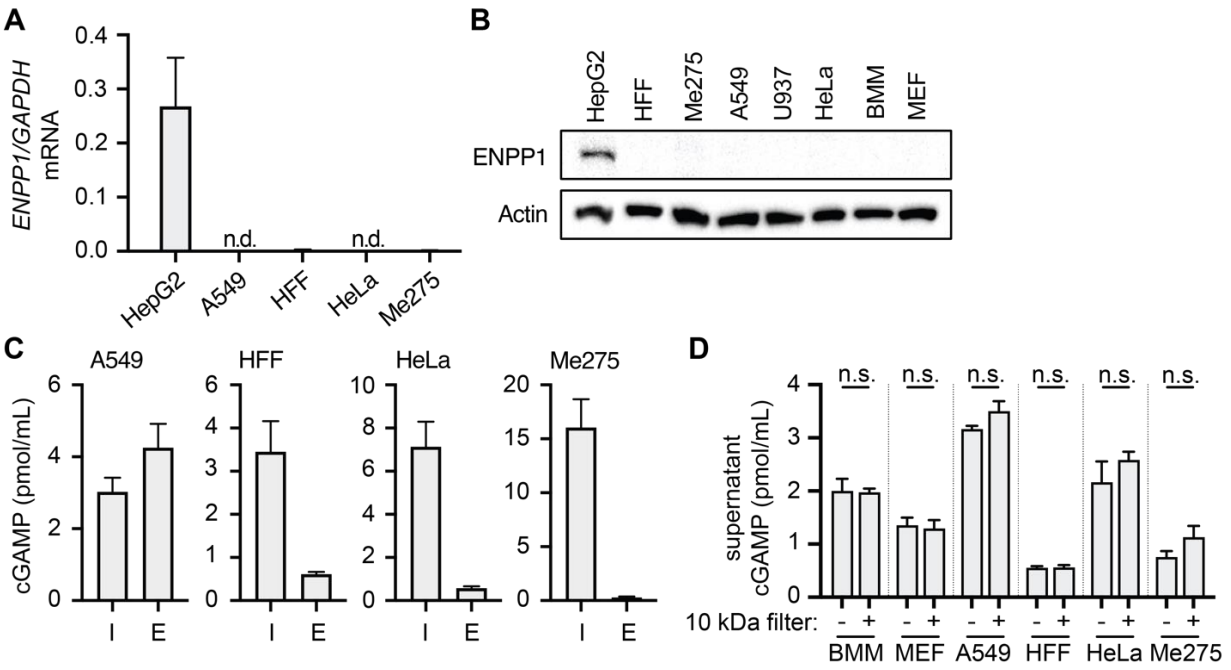

Figure 2.2: (A) Quantification of *ENPP1* mRNA transcript in indicated cell types by RT-qPCR. HepG2 cells are used as control for *ENPP1* expression. (B) Quantification of ENPP1 protein by Western blot. HepG2 cells are used as control for ENPP1 expression. (C) Quantification of intracellular and extracellular cGAMP from indicated cell types following CT DNA transfection for 8 hours. (D) Quantification of extracellular cGAMP pre (-) and post (+) filtration through a 10 kDa filter for exosome removal. Error bars represent mean ± SD. All data shown are derived from a single representative experiment. Comparative results were obtained across 3 independent experiments.

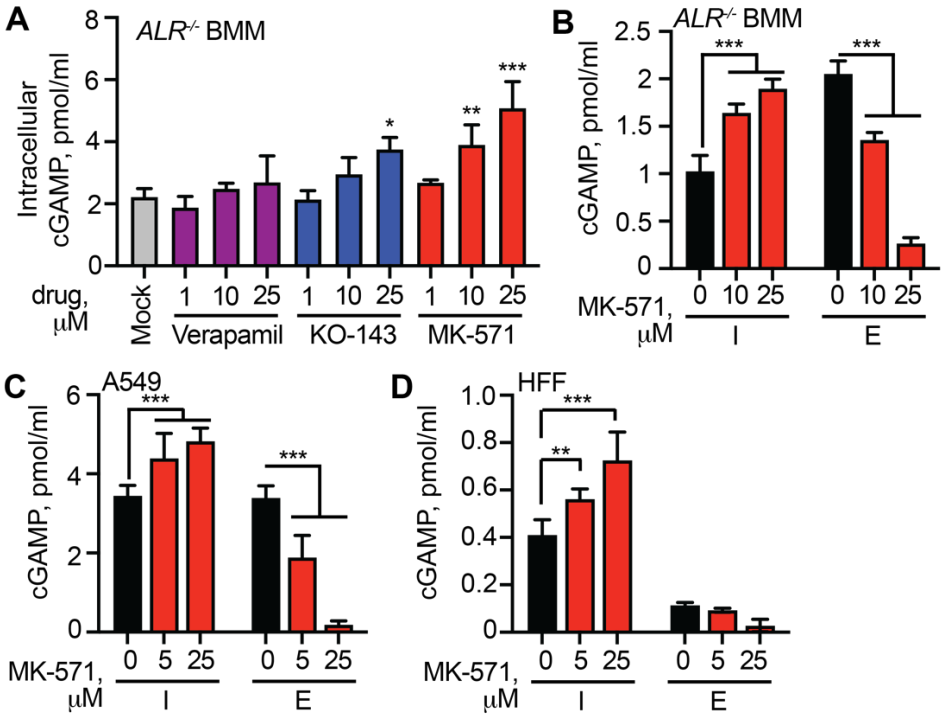

Figure 2.3: (A) ALR KO BMMs were treated with 1, 10, or 25 μM of indicated inhibitor or mock, followed by CT DNA transfection. 8 hours later, intracellular cGAMP was quantified in cell lysates using ELISA. (B) ALR KO BMMs were treated with 10 or 25 μM MK-571 or mock, followed by CT DNA transfection. 8 hours later, cell lysates and supernatants were harvested and cGAMP was quantified using ELISA (I: intracellular; E: extracellular). (C-E) Various human cell types were treated with MK-571 (2.5-50 μM) or mock, followed by CT DNA transfection. 8 hours later, cell lysates and supernatants were harvested and cGAMP was quantified using ELISA. Statistical analysis was performed using a one-way ANOVA comparing all drug treatments to mock (A, E) or a two-way ANOVA comparing drug treatments to mock-treated conditions in the intracellular or extracellular compartment (B-D). Tests corrected for multiple comparisons using the Holm-Sidak method. Error bars represent mean ± SD. **p<0.01, ***p<0.001. All data shown are derived from a single representative experiment. Comparative results were obtained across 2 (A, E) or 3 (B-D) independent experiments.

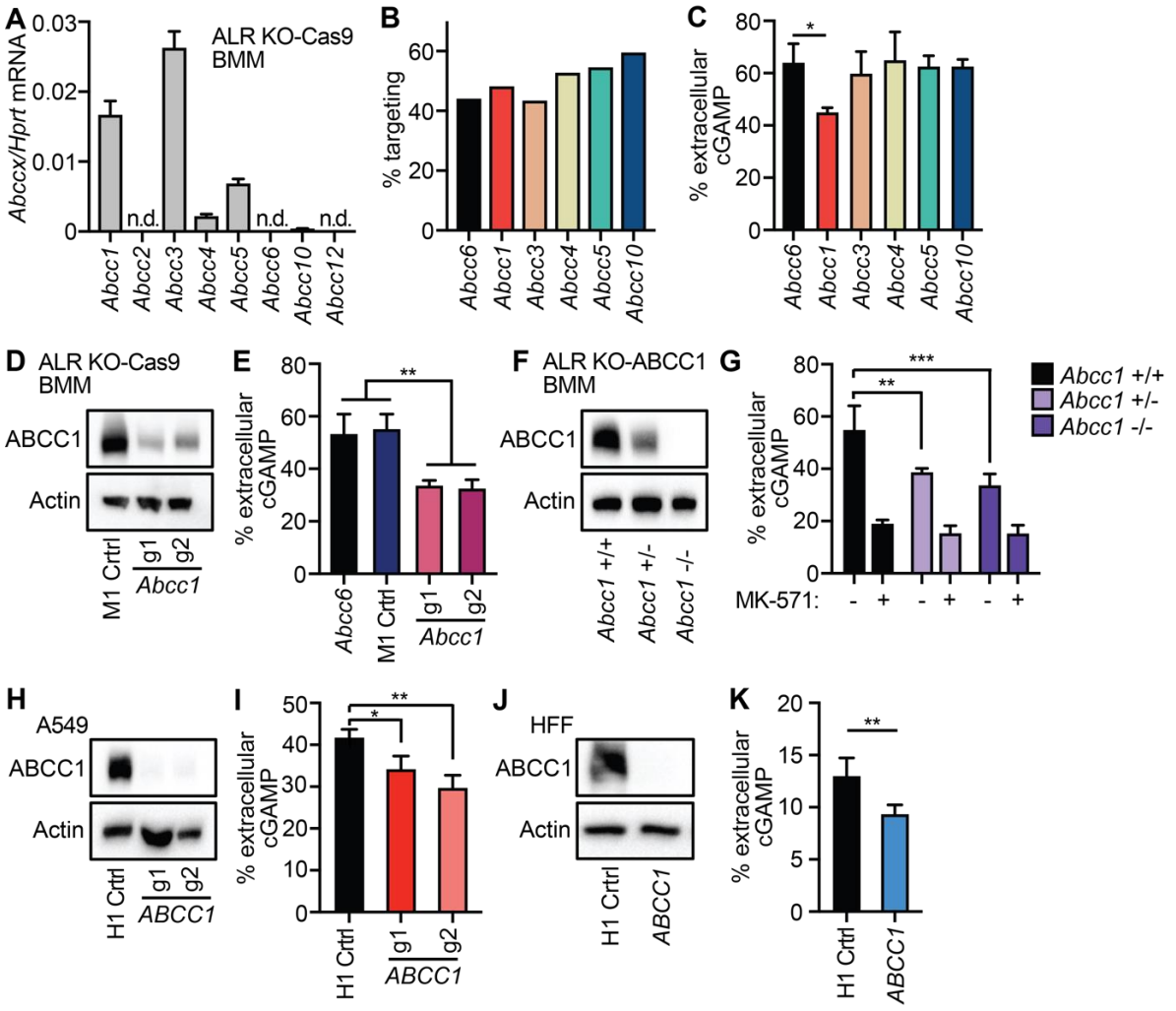

Figure 2.4: (A) Quantification of ABCC family member mRNA transcript expression in ALR KO-Cas9 BMMs by RT-qPCR. (B) ALR KO-Cas9 BMMs were transduced with lentiCRISPR encoding the indicated ABCC family-specific gRNAs, selected for 3 days, and then percent genomic targeting was calculated using Sanger sequencing and Tracking of Indels by DEcomposition (TIDE) analysis. (C) Cells from (B) were transfected with CT DNA and then 8 hours later cGAMP was quantified in supernatants and cell lysates using ELISA. (D) ALR KO-Cas9 BMMs were transduced with lentiCRISPR encoding *Abcc1* or M1 control-specific gRNAs as described in (B) followed by Western blot analysis for ABCC1 protein. (E) Cells from (D) were transfected with CT DNA and then 8 hours later cGAMP was quantified in supernatants and cell lysates using ELISA. (F) BMMs were harvested from ALR KO mice that were crossed to different ABCC1 genotypes and then evaluated by Western blot for ABCC1 protein. (G) Cells from (F) were transfected with CT DNA and then 8 hours later cGAMP was quantified in supernatants and cell lysates using ELISA. (H) A549 cells were transduced with lentiCRISPR encoding *ABCC1*- or H1 control-specific gRNAs as described in (B) and ABCC1 protein expression was evaluated by Western blot. (I) Cells from (H) were transfected with CT DNA and then 8 hours later cGAMP was quantified in supernatants and cell lysates using ELISA. (J) HFFs were transduced with lentiCRISPR encoding *ABCC1*- or H1 control-specific gRNAs as described in (B) and ABCC1 protein was assessed by Western blot. (K) Cells from (J) were transfected with CT DNA and then 8 hours later cGAMP was quantified in supernatants and cell lysates using ELISA. Statistical analysis was performed using a one-way ANOVA comparing targeted lines to relevant controls and corrected for multiple comparisons using the Holm-Sidak method. Error bars represent mean ± SD of 3 biological replicates per group. *p<0.05, **p<0.01, ***p<0.001. All data shown are derived from a single representative experiment. Comparative results were obtained across 2 (A-C, F, G) or 3 (D, E, H-K) independent experiments.

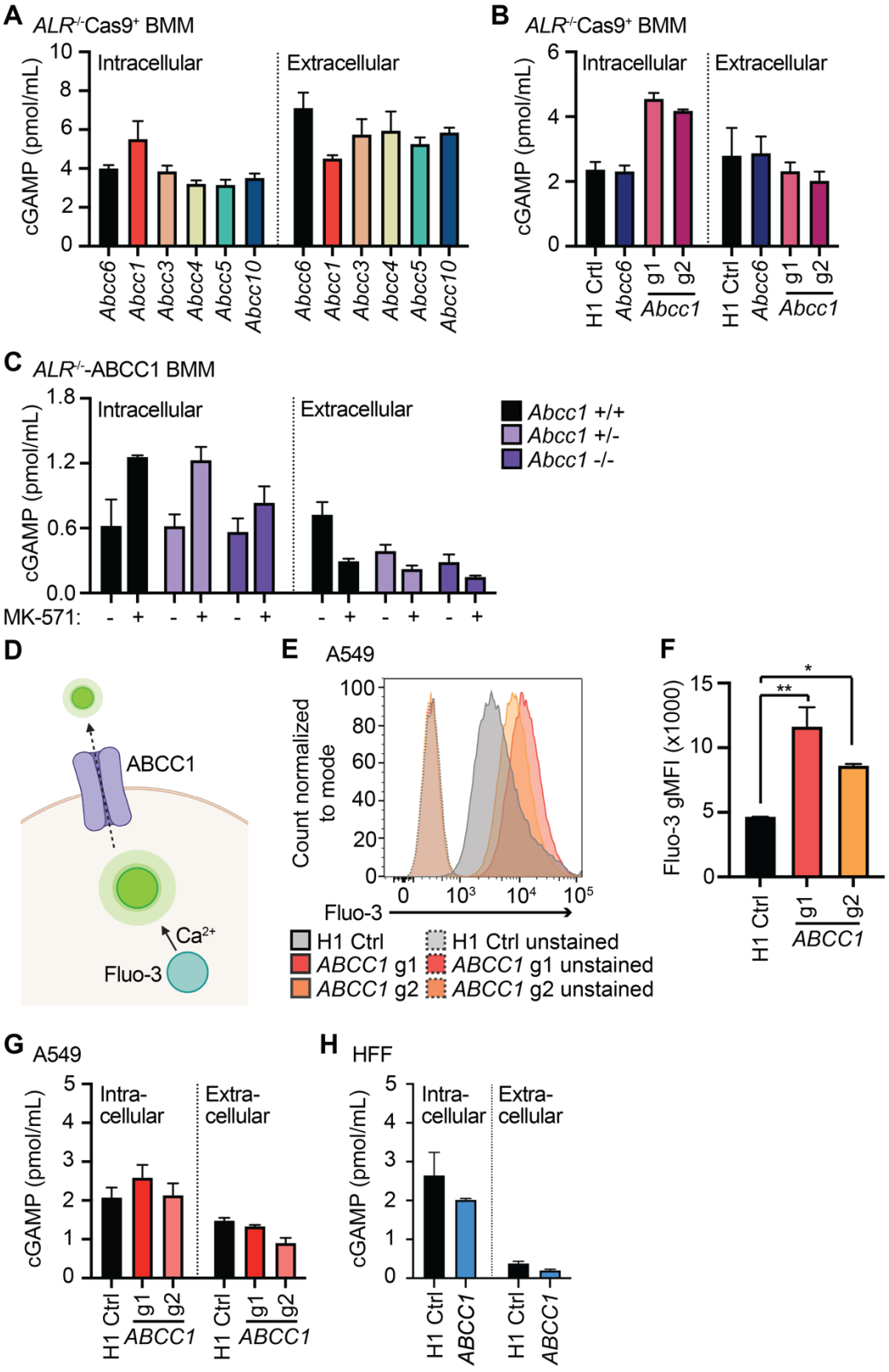

Figure 2.5: (A, B) Quantification of intracellular and extracellular cGAMP from indicated targeted lines of BMMs following CT DNA transfection for 8 hours. (C) Quantification of intracellular and extracellular cGAMP from indicated genotypes following CT DNA transfection for 8 hours. Cells were pretreated with

25 μM MK-571 or mock. (D) Schematic of Fluo-3AM staining and export. (E) *ABCC1*- or H1 control-targeted A549 cells were stained with Fluo-3AM and incubated for 1 hour at 37 C, followed by flow cytometric quantification of Fluo-3AM staining intensity. (F) gMFI quantification of flow cytometry data from (E). (G, H) Quantification of intracellular and extracellular cGAMP from indicated cell types following CT DNA transfection for 8 hours. Error bars represent mean ± SD. Statistical analysis was performed using a one-way ANOVA comparing all groups to H1 control and corrected for multiple comparisons using the Holm-Sidak method (E). *$p<0.05$, **$p<0.01$. All data shown are derived from a single representative experiment. Comparative results were obtained across 2 (C-E) or 3 (A, B, F, G) independent experiments.

Chapter 3: Molecular characterization of the putative cGAMP exporter ABCC1/MRP1

Introduction

ABCC1/MRP1 has a ubiquitous expression pattern across all tissues and cell types (Protein Atlas). This means that, hypothetically, all cells expressing cGAS (which is also expressed by most cell types) should have some capacity to export cGAMP following cGAS activation. We previously demonstrated that loss of ABCC1 expression via lentiCRISPR gene targeting reduced levels of cGAMP export. We therefore hypothesize that high expression of ABCC1 will correspondingly enhance levels of extracellular cGAMP. We will measure ABCC1 protein expression across cell lines and attempt to correlate this information with cGAMP export efficiencies. We will also test whether overexpression via lentiviral transduction to stably induce ABCC1 expression will lead to increased cGAMP export in various cell lines.

Importantly, we will test the ATP-dependency of ABCC1-mediated cGAMP export in two ways: first, we will clone a point mutation into the second nucleotide binding domain (NDB) of both mouse and human ABCC1 that is known to reduce ABCC1-mediated LTC4 transport by approximately 70%[77]. Second, to evaluate the biochemical mechanisms of cGAMP export, we will employ a well-described *in vitro* assay in the ABC transporter field that makes use of "inside-out" vesicle preparations[78] made from plasma membranes. These vesicles, prepared using a complex extraction and enrichment approach, result in an inverted topology of ABC transporters such that they transport substrates from the solution in which they are suspended into a membrane-bound compartment, allowing for more detailed analysis of kinetics of transport, including ATP-binding kinetics.

These studies will test for functional orthology between mouse and human ABCC1, together with the requirement for ATP hydrolysis for cGAMP export. Gain-of-function evidence for cGAMP export via ABCC1/MRP1, in addition to the "gold standard" vesicle transport assays for ABC transporters, will provide sufficient evidence that ABCC1 is a bona fide cGAMP exporter. More broadly, these experiments will provide a foundation for enhancing cGAMP

export from human tumor cells, which is important for triggering innate immune responses in tumor-infiltrating innate immune cells[34].

Results

ABCC1 overexpression enhances cGAMP export

We found that ABCC1 protein expression levels correlated well with the diverse efficiencies of cGAMP export that we identified among several mouse and human cell lines (Figure 3.2A, 3.2B). We therefore tested whether ABCC1 overexpression could increase cGAMP export in cells with lower endogenous ABCC1 expression. To do this, we transduced HFFs, which had relatively low ABCC1 expression and poor cGAMP export efficiency, with lentivirus encoding human ABCC1. To test the requirement for ATP hydrolysis in cGAMP export, we introduced a K1333M point mutation into the second nucleotide binding domain (NBD) of ABCC1 that is known to potently reduce ABCC1-mediated LTC4 transport[77]. After selection of transduced cells, we observed increased ABCC1 protein levels (Fig 3.1A) and decreased Fluo-3 retention in the ABCC1-overexpressing HFFs relative to those transduced with control lentivirus (Fig. 3.2C, 3.2D), demonstrating increased ABCC1 function. Surprisingly, HFFs expressing K1333M mutant ABCC1 also had a significantly lower Fluo-3 MFI than control HFFs, but not as low as HFFs overexpressing WT ABCC1 (Fig. 3.2C, 3.2D). To our knowledge, Fluo-3 fluorescence has never been studied in the context of the K1333M mutation, so it is possible that Fluo-3 export by ABCC1 is partially ATP-independent. We next tested these cells for cGAMP export after DNA transfection. We found that HFFs overexpressing WT ABCC1 exported more than triple the percent of extracellular cGAMP compared to controls (Fig. 3.1B, 3.2E). In contrast, the K1333M mutant failed to enhance cGAMP export (Fig. 3.1B, Fig. S3.2E).

To evaluate functional orthology between human and mouse ABCC1, we cloned the murine ABCC1 open reading frame into a lentiviral vector, as well as the corresponding K1330M NBD mutation[77]. We transduced HeLa cells, which, like HFFs, have relatively low endogenous ABCC1 expression and low efficiency of cGAMP export. After selection of transduced cells, we observed increased ABCC1 protein in HeLa cells expressing both the WT ABCC1 and the K1330M mutant relative to those transduced with control lentivirus (Fig. 3.1C). We transfected

these cells with CT DNA and found that HeLa cells overexpressing WT murine ABCC1, but not K1330M ABCC1, had a significant increase in the percent of extracellular cGAMP (Fig. 3.1D, Fig. 3.2F). Finally, we found that overexpression of either human or mouse ABCC1 significantly enhanced cGAMP export in Me275 human melanoma cells (Figure 3.1E, 3.1F, 3.2G), which were the poorest cGAMP exporters among the cell types we examined. Together, these data demonstrate that both human and mouse ABCC1 mediate ATP-dependent cGAMP export.

One potential caveat of our functional studies of cGAMP export in cells is the possibility that cGAMP is not a direct substrate of ABCC1, and that cGAMP export is instead stimulated indirectly by the movement of a distinct, unrelated ABCC1 substrate. We therefore performed biochemical assays to evaluate cGAMP transport using commercially available “inside out” vesicles prepared from Spodoptera frugiperda (fall armyworm Sf9) insect cells. These inside out vesicles are a “gold standard” in the biochemistry of transporters and have been used to define three broad classes of ABCC1 substrates: 1) molecules that are transported on their own, 2) molecules that are transported as covalent conjugates with glutathione, and 3) molecules that are co-transported with glutathione in the absence of covalent conjugation[59]. Using vesicles derived from Sf9 cells overexpressing human ABCC1, we found robust, ATP-dependent cGAMP transport that increased over time (Fig. 3.3A). We then focused on the 5- minute and 20-minute time points for more detailed analysis. At 5 minutes of incubation, we found that ABCC1-expressing vesicles transported cGAMP in the presence of ATP but not AMP, whereas control vesicles did not (Fig. 3.3B). In addition, we observed that ABCC1-expressing vesicles transported similar amounts of cGAMP in the presence or absence of glutathione (Figure 3.3B). Interestingly, at the 20-minute time point, we observed significant cGAMP transport into the control Sf9-derived vesicles that did not express human ABCC1 (Figure 3.3C). The amount of cGAMP transported into the control vesicles was significantly less than that transported into the ABCC1-expressing vesicles. However, this endogenous cGAMP transport was similar to the transport observed in ABCC1-expressing vesicles in that it required ATP and was glutathione-

independent (Figure 3.3C). We found that MK-571 inhibited cGAMP transport into both the ABCC1-expressing vesicles and the control vesicles (Figure 3.3C). These data provide biochemical evidence that ABCC1 mediates direct, ATP-dependent, glutathione-independent transport of cGAMP.

Discussion

In these studies, we demonstrated that ABCC1 mediates ATP-dependent cGAMP export. We found that overexpression of both human and mouse ABCC1 in a variety of cell types could enhance cGAMP export efficiency. We further demonstrated that the K1333M mutation specifically ablates cGAMP export, demonstrating that this process is ATP-dependent. Importantly, this is the first identified cGAMP transport mechanism that is energy dependent. Whereas the cGAMP importers (SLC19A1, SLC46A2, LRRC8:A-C) are all channels that operate via electrochemical gradient, transport of cGAMP by ABCC1 relies on the hydrolysis of two molecules of ATP and can therefore hypothetically export substrates against a concentration gradient.

We identified highly variable cGAMP export efficiencies across multiple human cancer cell lines, and these data demonstrate that ABCC1 overexpression converted poor cGAMP exporters (HFF, Me275) into more efficient exporters. Prior studies highlighted an essential role for tumor-derived extracellular cGAMP in priming antitumor immune responses[34, 35]. Our findings raise the interesting possibility that high expression of ABCC1 on tumor cells enhances antitumor immune responses through increased extracellular cGAMP in the tumor microenvironment. However, it is known that overexpression of ABCC1 by tumor cells renders them resistant to certain chemotherapeutic drugs that have been previously defined as export substrates of ABCC1[59]. Thus, the potential clinical utility of ABCC1 inhibitors in cancer patients to limit efflux of anti-cancer chemotherapeutics might be offset by their potential to reduce the export of an important innate immune signal that primes anti-tumor immunity. Therefore, our finding that cGAMP is a substrate of ABCC1 warrants further study of the consequences of ABCC1 blockade in cancer.

Finally, using inside out vesicles derived from Sf9 insect cells, we provide biochemical evidence that ABCC1 is a direct, ATP-dependent, glutathione-independent cGAMP transporter. These data suggest that cGAMP belongs to the class of ABCC1 substrates that are neither

conjugated to glutathione nor co-transported with glutathione[59]. Recent structural studies have identified a bipartite substrate binding site in ABCC1 comprised of a positively charged pocket that can bind the negatively charged glutathione moiety, together with a large hydrophobic pocket that can accommodate lipid moieties of glutathione-conjugated substrates like LTC4[79]. We propose that cGAMP engages the same positively charged pocket as gluthathione itself using its negatively charged phosphate groups, which would explain why cGAMP export does not require glutathione as a cofactor. Further biochemical and structural studies will provide additional insight into the cGAMP export mechanism by ABCC1. Furthermore, the discovery of pharmacologically similar cGAMP transport in plain Sf9 cell-derived vesicles at longer timepoints suggests that ATP-dependent cGAMP export is a conserved mechanism that exists in both arthropods and chordates. A detailed evolutionary analysis will shed further light into whether this is indeed a conserved mechanism of cGAMP export that spans ~700 million years of evolution since the divergence of arthropods and chordates.

Chapter 3 Figures

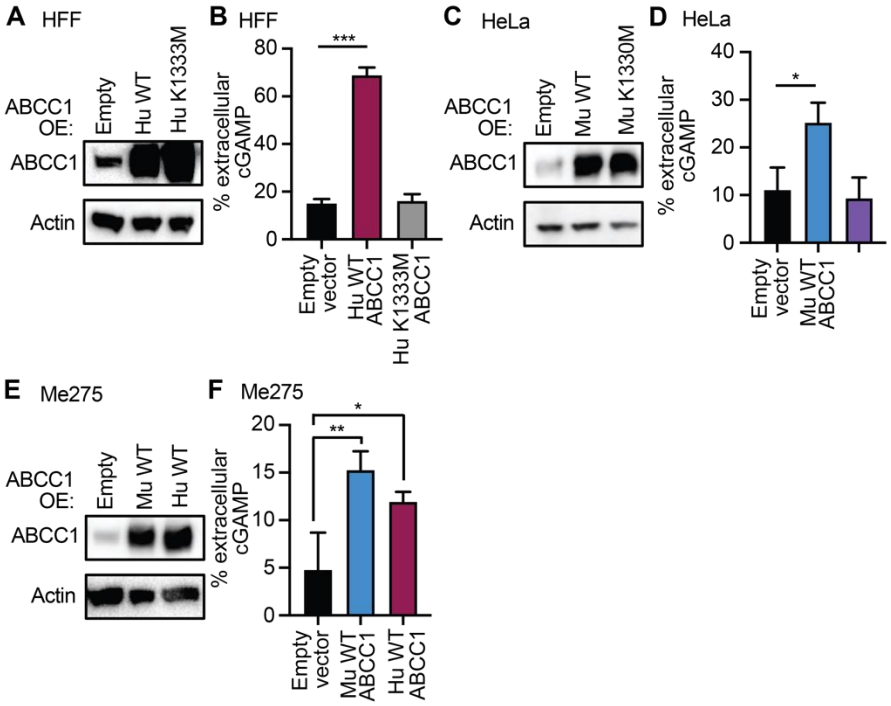

Figure 3.1: (A) HFFs were transduced with lentivirus encoding human WT or K1333M mutant ABCC1 or control (empty vector) and selected for 5 days in hygromycin. Cells were evaluated for ABCC1 protein expression by Western blot. (B) Cells from (A) were transfected with CT DNA and then 8 hours later cGAMP was quantified in supernatants and cell lysates using ELISA. (C) HeLa cells were transduced with lentivirus encoding murine WT or K1330M mutant ABCC1 or control (empty vector) and selected for 5 days in hygromycin. Cells were evaluated for ABCC1 protein expression by Western blot. (D) Cells from (C) were transfected with CT DNA and then 8 hours later cGAMP was quantified in supernatants and cell lysates using ELISA. (E) Me275 cells were transduced with lentivirus encoding human or murine WT ABCC1 or control (empty vector) and selected for 5 days in hygromycin. Cells were evaluated for ABCC1 protein expression by Western blot. (F) Cells from (E) were transfected with CT DNA and then 8 hours later cGAMP was quantified in supernatants and cell lysates using ELISA. Statistical analysis was performed using a one-way ANOVA comparing WT or mutant ABCC1-overexpression cells to empty vector control (B, D, F) and corrected for multiple comparisons using the Holm-Sidak method. Error bars represent mean ± SD of three biological replicates per group. *p<0.05, **p<0.01, ***p<0.001. All data shown are derived from a single representative experiment. Comparative results were obtained across three independent experiments.

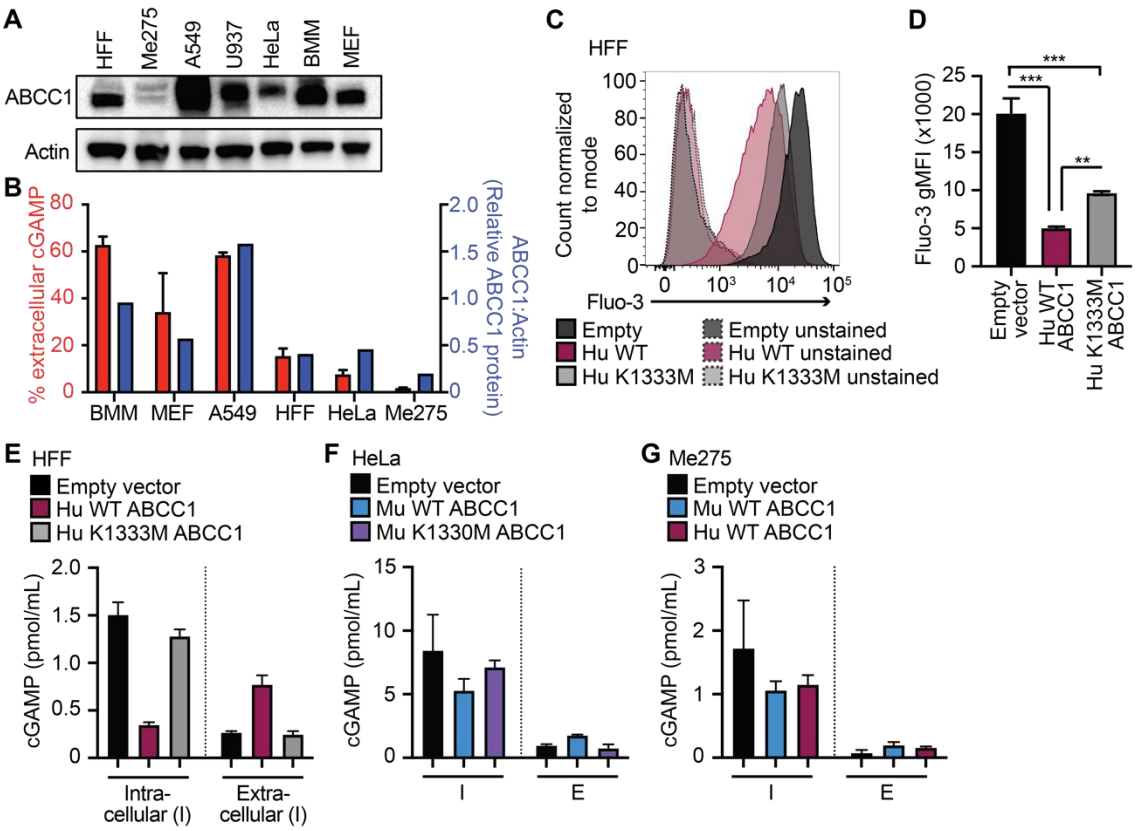

Figure 3.2: (A) Western blot analysis of indicated cells for ABCC1 protein expression. (B) cGAMP export efficiency calculated in Fig. 1E overlayed with densitometry from (A) for ABCC1 protein expression normalized to Actin expression. (C) HFFs were transduced with lentivirus encoding human WT or K1333M mutant ABCC1 or control (empty vector) and selected for 5 days in hygromycin. Cells were stained with Fluo-3AM and incubated for 1 hour at 37 C, followed by flow cytometric quantification of Fluo-3AM staining intensity. (D) Quantification of gMFI from (C). (E-G) Quantification of intracellular and extracellular cGAMP from indicated cell types following CT DNA transfection for 8 hours. Statistical analysis was performed using a one-way ANOVA comparing the means of all groups to each other (D) and corrected for multiple comparisons using the Holm-Sidak method. Error bars represent mean ± SD of three biological replicates per group. **p<0.01, ***p<0.001. All data shown are derived from a single representative experiment. Comparative results were obtained across three independent experiments.

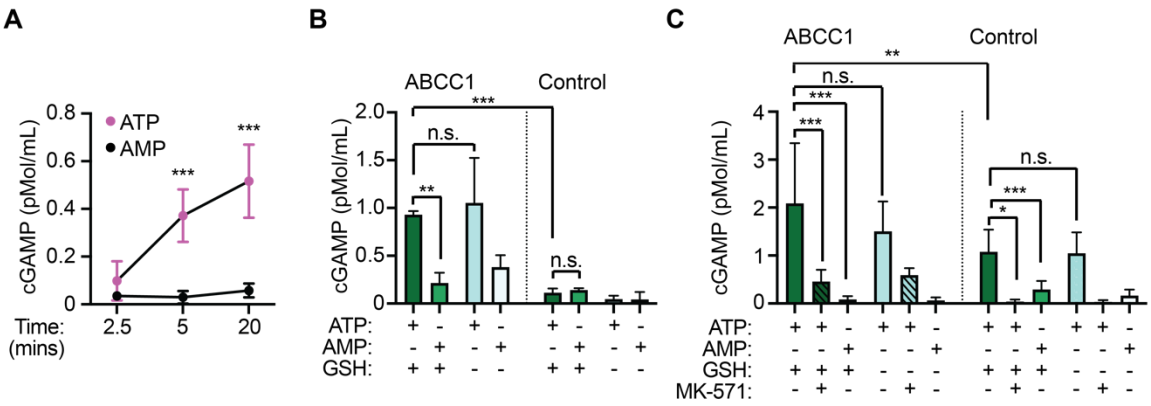

Figure 3.3: (A) Time course of cGAMP transport using Sf9 cell-derived vesicles expressing human ABCC1 in the presence of ATP or AMP. (B) 5-minute vesicle transport assays using Sf9 insect cell-derived vesicles expressing human ABCC1 or control vesicles with cGAMP in the presence of ATP or AMP, and with or without glutathione (GSH). (C) 20-minute vesicle transport assays using Sf9 insect cell-derived vesicles expressing human ABCC1 or control vesicles with cGAMP in the presence of ATP or AMP, with or without glutathione (GSH), and with or without MK-571 (25 mM). Statistical analysis was performed using one-way ANOVA comparing within time points (A) or comparing the mean of each group to every other group (B, C), and corrected for multiple comparisons using the Holm-Sidak method. Error bars represent the mean ± SD of 3-8 biological replicates per group. *p<0.05, **p<0.01, ***p<0.001. All data shown are derived from a single experiment. Comparative results were obtained across three (A, B) or two (C) independent experiments.

Chapter 4: ABCC1 negatively regulates cell-intrinsic STING signaling

Introduction

Having identified ABCC1 as an exporter of cGAMP, we next asked what effect the activity of ABCC1 might have on downstream STING signaling. Because cGAMP binds to and activates STING, we hypothesize that cGAMP export reduces cell-intrinsic STING signaling. However, extracellular cGAMP has also been described as an "immunotransmitter" that can be imported into bystander cells[35]. In this case, cGAMP export might serve to enhance STING signaling in the tissue microenvironment. We will therefore utilize both cell lines targeted for *ABCC1* as well as cell lines overexpressing ABCC1 to assess the contribution of ABCC1-mediated cGAMP export to STING signaling and IFN production. We will also perform DNA virus infections in these cell types to further assess the role of ABCC1 in controlling STING-dependent immune responses.

Whereas the cell-intrinsic effects of cGAMP export are straightforward to model in cell culture, the complex interactions between cells that produce cGAMP and cells that respond to extracellular cGAMP are difficult to model *in vitro*. We therefore plan to evaluate the contribution of ABCC1-mediated cGAMP export *in vivo* in a well-characterized mouse model of autoimmune disease. Mutations in the human gene that encodes the TREX1 DNA exonuclease cause a rare and severe autoimmune disease called Aicardi-Goutières Syndrome (AGS)[80]. We have shown that TREX1 is an essential and specific negative regulator of the cGAS-STING DNA sensing pathway[22]. *Trex1*$^{-/-}$ mice have a median life span of around 110 days and develop severe autoimmunity that requires cGAS[81, 82], STING[83], type I IFNs[22], and lymphocytes[22, 83]. Whereas *Trex1*$^{-/-}$ mice have been valuable to define key cells and signaling pathways that cause disease, no genetic modifiers that limit or restrict disease have yet been identified. We will utilize *Trex1*$^{-/-}$ mice to explore the contribution of cGAMP export in a clinically relevant mouse model of human autoimmunity. We will generate *Abcc1*$^{+/+}$*Trex1*$^{-/-}$ and *Abcc1*$^{-/-}$*Trex1*$^{-/-}$ mice and controls and compare their survival. If genetic disruption of ABCC1-mediated cGAMP enhances STING

signaling, we expect accelerated mortality in *Abcc1*$^{-/-}$*Trex1*$^{-/-}$ mice. However, if ABCC1-mediated cGAMP export is important for disseminating innate immune signals that are important for disease, we predict that the *Abcc1*$^{-/-}$*Trex1*$^{-/-}$ mice would be protected from mortality. Importantly, we have identified conditions of partial rescue and delayed mortality in *Trex1*$^{-/-}$ mice in the past, particularly in the context of mice heterozygous for *Irf3* and *Cgas*[22, 81], demonstrating that this model is suitable to detect more subtle changes in the course of disease.

Results

Modulation of cGAMP export influences cell-intrinsic STING signaling

cGAMP binding to STING activates TBK1- and IRF3-dependent transcription of type I interferon genes[84]. We hypothesized that reduction of intracellular cGAMP concentrations through ABCC1-dependent export would similarly reduce cell-intrinsic STING signaling. Consistent with this hypothesis, we found that pretreatment of HFFs with MK-571 potently enhanced DNA-activated *IFNB1* transcription but not RNA-activated *IFNB1* transcription (Fig. 4.1A). Similarly, MK-571 pretreatment enhanced the response in cells treated with extracellular cGAMP, as evidenced by enhanced phospho-STING and phospho-IRF3 protein (Fig. 4.1B), as well as increased *IFNB1* transcription (Fig. 4.1C). These data demonstrate that cGAMP export limits cell intrinsic STING signaling and enhances the stimulatory activity of imported cGAMP.

Given our findings that pharmacological blockade of cGAMP export enhanced STING signaling, we hypothesized that modulation of ABCC1 expression alters Type I IFN production. To test this, we stimulated our ABCC1-overexpressing HFFs (Fig. 3.1A, 3.1B) with CT DNA and found that these cells had significantly lower *IFNB1* transcript levels compared to control cells throughout a 6-hour time course (Fig. 4.1D). Within this same experiment, we found decreased phospho-STING at each time point in ABCC1-overexpressing cells, consistent with the reduction in Type I IFN levels (Fig. 4.1E). Conversely, we found that DNA-stimulated HFFs targeted for *ABCC1* with lentiCRISPR (Fig. 2.4J, 2.4K) had increased *IFNB1* transcript levels and accelerated kinetics of phospho-STING protein when compared to H1 non-targeting control cells (Fig. 4.1F, 4.1G). These findings demonstrate that modulation of ABCC1 expression alters the antiviral response to DNA and suggest that ABCC1 acts as a negative regulator of cell intrinsic STING signaling.

Loss of cGAMP export protects cells from DNA virus infection

Following up on our finding that loss of cGAMP export leads to accelerated phospho-STING signaling kinetics and subsequent enhanced Type I IFN production, we next asked

whether this phenotype would be protective against DNA virus infection. We found that ALR-KO, *Abcc1*$^{-/-}$ BMMs infected with HSV-1 KOS strain at varying multiplicities of infection (MOI) were more protected from viral infection and replication than control ALR-KO, *Abcc1*$^{+/+}$ cells, as measured by expression of the viral-derived ICP0 protein (Fig. 4.2A). We expected this to be due to enhanced Type I IFN and elevated ISGs, as seen in the *ABCC1* lentiCRISPR-targeted HFFs. However, we noted that at the two time points tested, both *Ifnb1* transcript as well as ISG transcripts were decreased in *Abcc1*$^{-/-}$ BMMs (Fig. 4.2B). We expect this is due to an early initial burst of Type I IFN produced by the cells upon infection, as the *ABCC1* lentiCRISPR-targeted HFFs had significantly stronger phospho-STING signaling as early as two hours after transfection with CT-DNA when compared with control cells. However, further studies are needed to better evaluate this phenotype. We emphasize that restriction of HSV-1 replication is in line with our hypothesis that ABCC1-deficient cells are more resistant to viral infection due to elevated intracellular cGAMP. *Abcc1*$^{-/-}$*Trex1*$^{-/-}$

ABCC1 deficiency enhances cGAS-dependent autoimmunity in Trex1$^{-/-}$ *mice*

Since ABCC1 expression correlated negatively with type I IFN production after DNA stimulation (Fig. 4.1), we hypothesized that loss of ABCC1 in *Trex1*$^{-/-}$ mice would lead to accelerated mortality from enhanced IFN-mediated disease. We intercrossed *Trex1*$^{-/-}$ and *Abcc1*$^{-/-}$ mice and monitored survival. We found that both *Abcc1*$^{-/-}$*Trex1*$^{-/-}$ and *Abcc1*$^{+/-}$*Trex1*$^{-/-}$ mice exhibited significantly accelerated mortality compared to *Abcc1*$^{+/+}$*Trex1*$^{-/-}$ mice (Fig. 4.3A). The accelerated mortality of *Trex1*$^{-/-}$ mice on both *Abcc1*$^{+/-}$ and *Abcc1*$^{-/-}$ backgrounds was consistent with the similarly reduced cGAMP export in both *Abcc1*$^{+/-}$ and *Abcc1*$^{-/-}$ BMMs (Fig. 2.4G), suggesting that haploinsufficiency for Abcc1 is sufficient to modify the course of disease. At 35 days of age *Abcc1*$^{-/-}$*Trex1*$^{-/-}$ mice were more severely runted than *Abcc1*$^{+/+}$*Trex1*$^{-/-}$ mice (Fig. 4.3B). We measured tissue cGAMP levels and found that hearts from over half of the *Abcc1*$^{-/-}$ mice that we sampled had detectable levels of cGAMP, whereas we could not detect cGAMP in heart tissue from any *Abcc1*$^{+/+}$ (WT) mice or from *Cgas*$^{-/-}$ mice that served as a

negative control for the assay (Fig. 4.3C). This increase is consistent with previously reported steady state accumulation of glutathione (a distinct ABCC1 substrate) in hearts of *Abcc1*$^{-/-}$ mice[85]. Heart cGAMP levels were detectable in most *Abcc1*$^{+/+}$*Trex1*$^{-/-}$ mice and significantly increased in all *Abcc1*$^{-/-}$*Trex1*$^{-/-}$ mice relative to control mice (Fig. 4.3C). Despite the limit of detection of the cGAMP ELISA assay, these data suggest that ABCC1 deficiency results in increased tissue cGAMP levels in both steady state and during cGAS-dependent disease. We evaluated the serum protein levels of the IFN-dependent chemokine CXCL10 and found that CXCL10 was significantly elevated in *Abcc1*$^{-/-}$*Trex1*$^{-/-}$ mice compared to *Abcc1*$^{+/+}$*Trex1*$^{-/-}$ mice (Fig. 3.4D). Similarly, *Isg15* mRNA expression levels in heart tissue were significantly higher in *Abcc1*$^{-/-}$*Trex1*$^{-/-}$ mice compared to *Abcc1*$^{+/+}$*Trex1*$^{-/-}$ mice, consistent with enhanced IFN signaling (Fig. 4.3E). We next prepared BMMs from age- and sex-matched mice and found that expression of *Ifnb1* mRNA was significantly increased in *Abcc1*$^{-/-}$*Trex1*$^{-/-}$ BMMs compared to *Abcc1*$^{+/+}$*Trex1*$^{-/-}$ BMMs (Fig. 4.3F), suggesting that loss of ABCC1 enhances the spontaneous type I IFN response caused by Trex1 deficiency.

Lastly, we performed a blinded histological analysis of affected tissues, comparing *Abcc1*$^{-/-}$*Trex1*$^{-/-}$ mice and *Abcc1*$^{+/+}$*Trex1*$^{-/-}$ mice to *Abcc1*$^{-/-}$ controls. While we observed a trend towards more severe heart pathology in *Abcc1*$^{-/-}$*Trex1*$^{-/-}$ mice compared to *Abcc1*$^{+/+}$*Trex1*$^{-/-}$ mice, this did not reach statistical significance in the context of our scoring criteria, likely because of the severe inflammation that has been well documented in the plain *Trex1*$^{-/-}$ hearts (Fig 4.3G, 4.3H). We also noted the presence of focal to multifocal, generally mild, perivascular lymphoid aggregates (with lower numbers of other inflammatory cells) associated with the meninges and periosteum of the skull in 3/4 *Abcc1*$^{-/-}$*Trex1*$^{-/-}$ mice compared to 1/4 *Abcc1*$^{+/+}$*Trex1*$^{-/-}$ mice (Fig. 4.3H). Taken together, these data suggest that ABCC1 is a genetic modifier and negative regulator of the cGAS-cGAMP-STING pathway in vivo in a model of chronic cGAS activation.

Discussion

Our findings have important implications for our understanding of the regulatory mechanisms involved in cGAS-STING signaling. We demonstrate that genetic ablation or pharmacological blockade of ABCC1 enhances cell-intrinsic STING signaling, whereas overexpression of ABCC1 reduces STING signaling. Thus, by limiting intracellular cGAMP concentrations, ABCC1 negatively regulates the cGAS-STING pathway and provides a mechanism to expose extracellular cGAMP to ENPP1-mediated degradation[86]. In line with this, ABCC1-deficient cells were more resistant to viral infection that control cells. Additionally, loss of *Abcc1* in the *Trex1*$^{-/-}$ mouse model led to accelerated and exacerbated disease, demonstrating that cGAMP export in this model serves to limit cell-intrinsic STING activation. Thus, ABCC1 is a genetic modifier that limits cGAS-dependent immune disease.

There are numerous polymorphisms in the human ABCC1 gene that have been associated with the varied responses to anthracycline-based chemotherapies in cancer patients[59]. It will be interesting to determine whether these or other ABCC1 polymorphisms influence the efficiency of cGAMP export and the strength of cGAS-STING signaling. We speculate that hypomorphic ABCC1 alleles might be evolutionarily advantageous because they provide superior protection against certain virus infections, but these same alleles might predispose to cGAS-dependent autoimmune disease. Because haploinsufficiency for *Abcc1* is sufficient to exacerbate disease in *Trex1*$^{-/-}$ mice (Fig. 4.3), we propose that subtle differences in expression levels and function of ABCC1 might have a significant impact on STING-dependent immunity.

Our studies did not directly test the “immunotransmitter” function of cGAMP signaling that is additionally regulated by cGAMP degradation and cGAMP import. Ultimately, the influence of cGAMP export on STING signaling could be context and disease dependent, and it is possible that ABCC1-mediated export can play a positive regulatory role in propagating STING signaling to bystander cells. For example, in earlier work we highlight the ability of

overexpression of ABCC1 to enhance export of cGAMP. In the context of the tumor microenvironment, we expect this to enhance antitumor immunity through increased import of cGAMP, which could give a beneficial increase in Type I IFN production.

In summary, we have identified ABCC1 as an important molecular site of action for cGAMP export. Our discovery highlights ABCC1 as a negative regulator of cell-intrinsic STING signaling and completes the cycle of cGAMP production, export, and import, further rationalizing the existence of an extracellular cGAMP degradation mechanism. Further investigation into ABCC1-mediated cGAMP export has the potential to yield novel therapeutic approaches to enhance the protective functions of type I IFN in human diseases.

Chapter 4 Figures

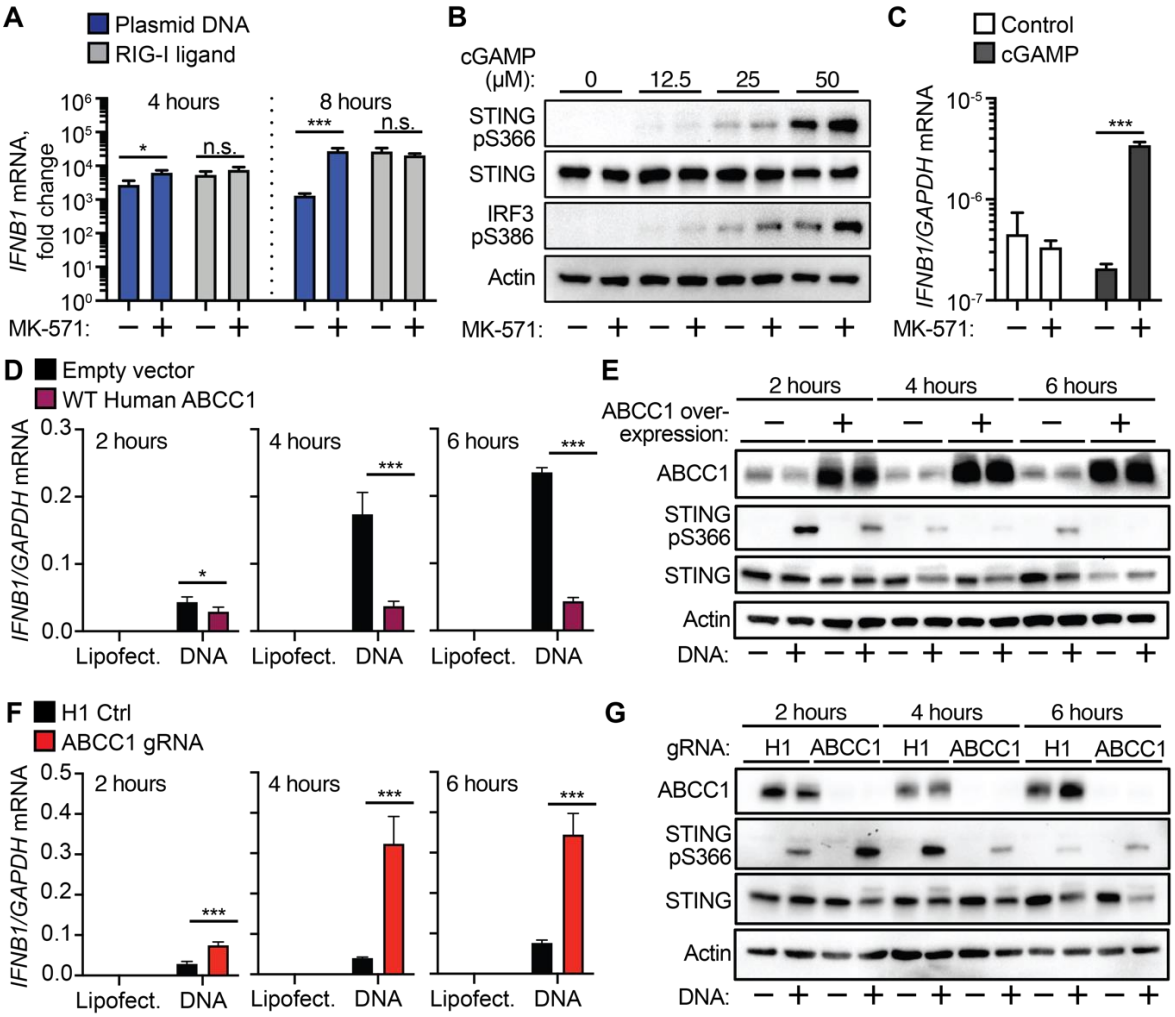

Figure 4.1: (A) Quantification of *IFNB1* induction by RT-qPCR in HFFs that were treated with 25 μM MK-571 or mock followed by transfection with plasmid DNA or RIG-I ligand for 4 or 8 hrs. (B) HFFs were treated with 25 μM MK-571 or mock, and then cGAMP (0-50 μM) was added to the extracellular media. Western blot analysis was performed 4 hours after cGAMP addition for phosphorylated STING, STING, and phosphorylated IRF3. (C) HFFs were treated with 25 μM MK-571 or mock, and then cGAMP (0 or 50 μM) was added to the extracellular media. *INFB1* induction was quantified by RT-qPCR 4 hours after cGAMP addition. (D) Quantification of *IFNB1* induction by RT-qPCR in HFFs overexpressing ABCC1 or empty vector control following transfection with CT DNA. Cells were harvested at the indicated time points. (E) Western blot analysis of cells from (D) for ABCC1, phosphorylated STING, and STING protein expression. (F) Quantification of *IFNB1* induction by RT-qPCR in *ABCC1*- or H1 control-targeted HFFs following transfection with CT DNA. Cells were harvested at the indicated time points. (G) Western blot analysis of cells from (F) for ABCC1, phosphorylated STING, and STING protein expression. Statistical analysis was performed using a two-way ANOVA comparing mock or MK-571 treatment within each transfected ligand group (A, C) or comparing control to ABCC1-modulated cells within each transfected ligand group (D, F). All tests were corrected for multiple comparisons using the Holm-Sidak method. Error bars represent mean ± SD. *p<0.05, ***p<0.001. All data shown are derived from a single representative experiment. Comparative results were obtained across 3 independent experiments.

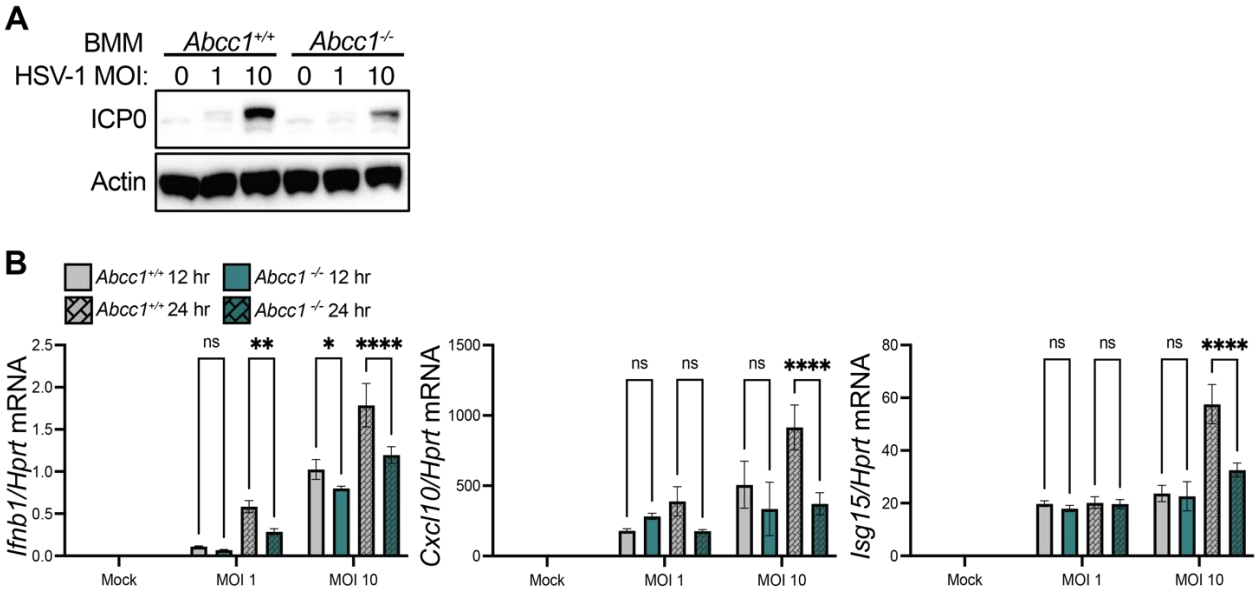

Figure 4.2: (A) Western blot analysis of HSV-1 ICP0 24 hours after ALR KO BMMs of the indicated genotypes were infected with HSV-1 at an MOI of 0, 1, or 10. (B) Quantification of *Ifnb1*, *Cxcl10*, and *Isg15* by RT-qPCR from cells treated as in (A) at 12 or 24 hours after infection. Statistical analysis was performed using a one-way ANOVA comparing gene expression across genotypes and time points (B). All tests were corrected for multiple comparisons using the Holm-Sidak method. Error bars represent mean ± SD of three biological replicates per group. *p<0.05, **p<0.01, ***p<0.001. All data shown are derived from a single representative experiment. Comparative results were obtained across three independent experiments.

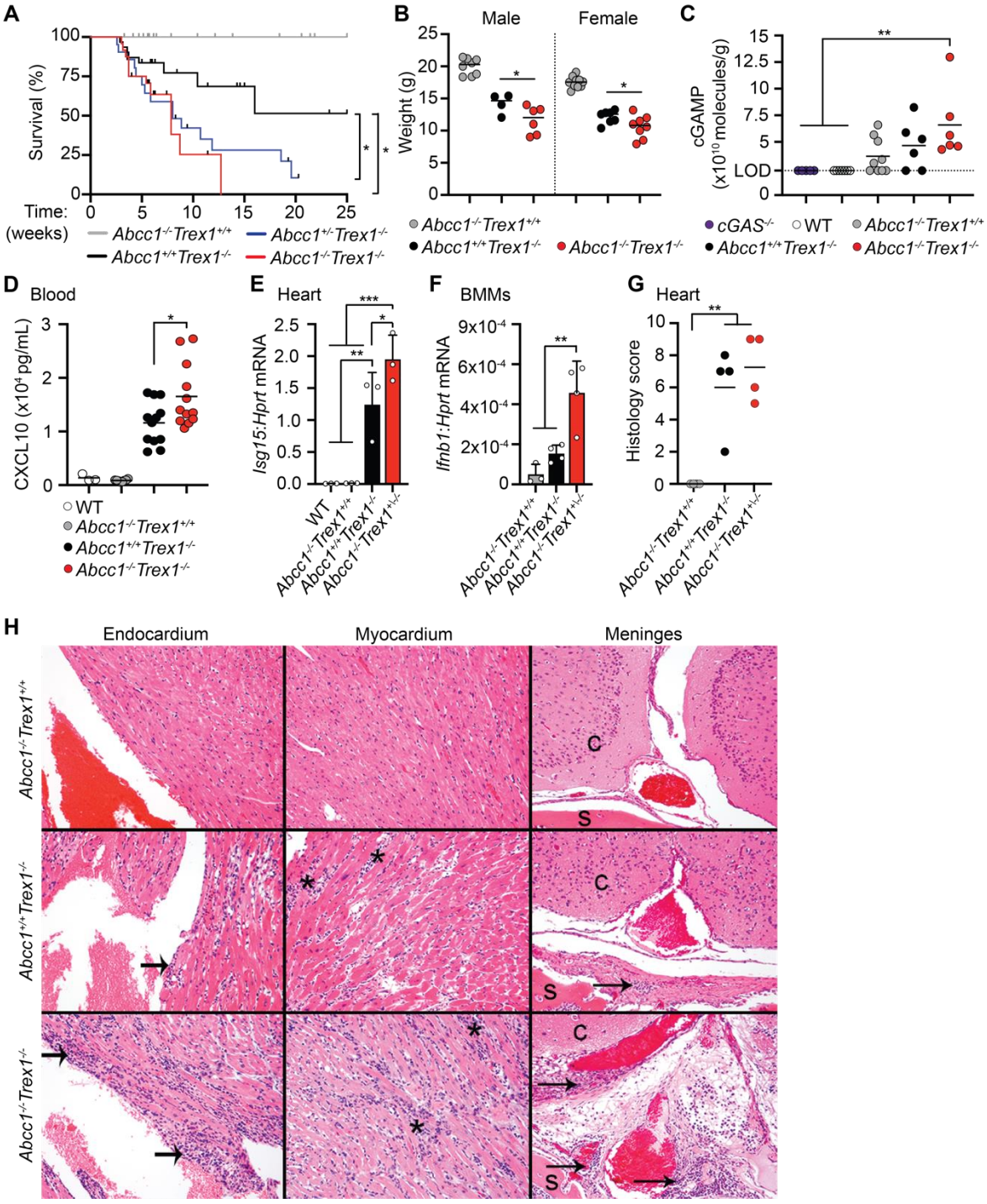

Figure 4.3: (A) Survival of *Abcc1*$^{-/-}$*Trex1*$^{+/+}$ (n= 33), *Abcc1*$^{+/+}$*Trex1*$^{-/-}$ (n= 31), *Abcc1*$^{+/-}$*Trex1*$^{-/-}$ (n= 21), and *Abcc1*$^{-/-}$*Trex1*$^{-/-}$ (n= 24) mice. (B) Weights of mice at 35 days of age; *Abcc1*$^{+/+}$*Trex1*$^{-/-}$ (n= 8 M, 10 F), *Abcc1*$^{+/+}$*Trex1*$^{-/-}$ (n= 4 M, 7 F), and *Abcc1*$^{-/-}$*Trex1*$^{-/-}$ (n= 6 M, 8 F). (C) Quantification of intracellular cGAMP recovered from heart tissue by ELISA; *Cgas*$^{-/-}$ (n= 5), WT (n= 7), *Abcc1*$^{-/-}$*Trex1*$^{+/+}$ (n= 9), *Abcc1*$^{+/+}$*Trex1*$^{-/-}$ (n= 6), *Abcc1*$^{-/-}$*Trex1*$^{-/-}$ (n= 6). Values are normalized to individual heart weights (LOD = limit of detection at 2.3x10^{10} molecules/g). (D) Quantification of Cxcl10 protein in serum measured by ELISA of the indicated genotypes; WT (n= 3), *Abcc1*$^{-/-}$ (n= 8), *Abcc1*$^{+/+}$*Trex1*$^{-/-}$ (n= 12), *Abcc1*$^{-/-}$*Trex1*$^{-/-}$ (n= 12). (E) Quantification of *Isg15* mRNA transcript levels by RT-qPCR in heart tissue of the indicated genotypes; n=

3 mice per group. (F) Quantification of *Ifnb1* mRNA transcript levels by RT-qPCR in BMMs of the indicated genotypes; n= 3 or 4 mice per group. (G) Histological score in heart tissue measured at 40 days of age; n= 4 mice per group. (H) Representative (of 4 of each genotype) H&E-stained heart (endocardium and myocardium) and brain at the level of cerebrum (c) with meninges, periosteum, and skull (s) tissue sections from *Abcc1*$^{-/-}$*Trex1*$^{+/+}$, *Abcc1*$^{+/+}$*Trex1*$^{-/-}$, and *Abcc1*$^{-/-}$*Trex1*$^{-/-}$ mice. *Abcc1*$^{+/+}$*Trex1*$^{-/-}$ and *Abcc1*$^{-/-}$ *Trex1*$^{-/-}$ mice have inflammation extending along the endocardial surface (wide arrows), which appears more pronounced in *Abcc1*$^{-/-}$*Trex1*$^{-/-}$ mice. *Abcc1*$^{+/+}$*Trex1*$^{-/-}$ and *Abcc1*$^{-/-}$*Trex1*$^{-/-}$ mice both have myocardial inflammation (asterisks) with variably severe myocardial degeneration. *Abcc1*$^{+/+}$*Trex1*$^{-/-}$ and *Abcc1*$^{-/-}$*Trex1*$^{-/-}$ mice have perivascular lymphocytic infiltrates (narrow arrows) in the meninges and periosteum of the skull which is variably severe and not present in all mice, but which is generally minimal in the *Abcc1*$^{+/+}$*Trex1*$^{-/-}$ mice. Statistical analysis for the survival curves was calculated with a log-rank (Mantel-Cox) test (A). Statistical analysis for all other experiments was performed using a one-way ANOVA comparing each group to every other group (C, D), comparing transcript level of each gene between genotypes (E, F), or comparing *Abcc1*$^{-/-}$*Trex1*$^{+/+}$ to *Abcc1*$^{+/+}$*Trex1*$^{-/-}$ and *Abcc1*$^{-/-}$*Trex1*$^{-/-}$ mice in (G). All ANOVA tests were corrected for multiple comparisons using the Holm-Sidak method. Error bars represent mean ± SD. The ROUT method was used to detect potential outliers and no outliers were detected across the data shown. *p<0.05, **p<0.01, ***p<0.001.

Chapter 5: Methods

Mice

ALR$^{-/-}$*, Sting (Tmem173)*$^{-/-}$*,* and *Trex1*$^{-/-}$ mice have been described[49, 83, 87]. C57BL/6J wild-type (stock #000664) and *Abcc1*$^{-/-}$ (stock #028129) mice were purchased from Jackson Laboratories. All mice used in this study were C57BL/6J and housed in a specific pathogen-free facility at the University of Washington with approval of the University of Washington Institutional Animal Care and Use Committee.

Cell lines and tissue culture

Primary mouse BMMs and MEFs were derived and cultured as previously described[64]. HeLa, U937, A549, and HepG2 were purchased from ATCC. Me275 cells, established at the Ludwig Institute for Cancer Research[53], were provided by A. Rongvaux (Fred Hutchinson Cancer Research Center). Telomerase-immortalized human foreskin fibroblasts (HFFs) were provided by D. Galloway (Fred Hutchinson Cancer Research Center). All adherent cell lines were cultured in DMEM supplemented with 10% FCS, L-glutamine, penicillin/streptomycin, sodium pyruvate, and HEPES. U937 cells were grown in RPMI supplemented as above and differentiated prior to stimulation using 100 nM phorbol myristoyl acetate for 24 hours and then rested in media for an additional 24 hours without PMA prior to treatment.

Quantification of cell death

BMMs and MEFs were seeded at a density of $2x10^4$ and $1x10^4$, respectively, in a 24-well plate. Cell death was assayed with a 2-color IncuCyte Zoom in-incubator imaging system (Essen Biosciences, Ann Arbor, MI, USA) and analyzed as described[88]. SytoxGreen and SytoGreen (25 nM, Life Technologies) were used to calculate the frequency of dead cells.

cGAMP measurements

For *in vitro* measurements, extracellular cGAMP was measured directly from cell supernatants that were maintained at a volume of 200 µL. To quantify intracellular cGAMP, cells were washed once with PBS and then lysed in 200 µL RIPA buffer (150 mM NaCl, 1% Triton-X-100, 0.5% sodium deoxycholate, 0.1% SDS, 50 mM Tris pH 8.0) for 15 minutes on ice. Lysates were then cleared of insoluble material before being used for cGAMP measurement. Relative cGAMP measurements were quantified using Direct 2'3'-Cyclic GAMP ELISA Kit (Arbor Assays).

To quantify cGAMP in mouse heart tissues, hearts were cleaned and weighed, minced, and then digested in dissociation buffer (2.7 mg/mL Collagenase A (Sigma), 23 U/mL DNase I (Sigma), 2 mM $CaCl_2$ in PBS) for 1 hour at 37º C. Digestion was terminated with termination buffer (2% FBS, 5 mM EDTA in PBS). Samples were strained through 70 µm mesh strainers, centrifuged, and then subjected to red blood cell lysis in buffer (150 mM NH_4CL, 10 mM $KHCO_3$, 0.1 mM Na EDTA in water). Remaining cells were washed twice and suspended in 200 µL RIPA buffer for 15 minutes of lysis, then centrifuged to clear of insoluble material before direct measurement in cGAMP ELISA Kit. Limit of detection (LOD) was calculated by averaging the weights of all control (*cGAS*$^{-/-}$ and *Abcc1*$^{-/-}$) hearts to use in calculation of molecules per gram of tissue with the given LOD of the ELISA Kit (0.04 pMol/mL).

Cell treatments and stimulations

For all *in vitro* experiments, cells were seeded in triplicate at a density of $1x10^5$ (A549, HeLa, Me275), $2x10^5$ (U937), or $2.5x10^4$ (HFFs) cells per well in 24-well plates. For nucleic acid transfections, calf thymus genomic DNA (Sigma) was diluted in water and used at 4 µg/mL (for human cells) or 1 µg/mL (for mouse cells); RIG-I ligand was synthesized *in vitro* as previously described using HiScribe T7 High Yield RNA Synthesis Kit[89] and used at 1 µg/mL; midiprepped pcDNA3 was used for plasmid stimulations at 4 µg/mL. For all transfections, nucleic acids were complexed with Lipofectamine 2000 (Invitrogen) at a ratio of 1 µg nucleic acid to 1 µL lipid. 2'3'

cGAMP (Invivogen) was diluted in water and directly added to cell culture media at 12.5 – 50 μM. MK-571, Verapamil, and KO-143 (Sigma) were suspended in DMSO and used to treat cells at concentrations from 1-50 μM for 1 hour prior to stimulation. Mock-treated cells received the same amounts of plain DMSO.

Western blotting and antibodies

Cells were harvested in RIPA lysis buffer supplemented with phosphatase and protease inhibitors (Pierce). Lysates were vortexed and incubated on ice for 15 minutes followed by clearing by centrifugation for 15 minutes. Proteins were separated on 4-12% Bis-Tris SDS-PAGE gel (Life Technologies) and transferred to Immobilon-P PVDF membrane (Millipore). Blots were blocked in 5% BSA/TBST or 5% non-fat dry milk depending on primary antibody used. Membranes were probed overnight at 4º C with the following primary antibodies: anti-mouse/human ABCC1 (Abcam ab260038), anti-mouse/human Actin (Cell Signaling #3700), anti-human phospho-STING (Cell Signaling #19781), anti-mouse phospho-STING (Cell Signaling #72971), anti-mouse/human STING (Cell Signaling #13647), anti-human phospho-IRF3 (Abcam ab196035). Membranes were then probed with goat anti-rabbit-HRP or goat anti-mouse-HRP (Jackson ImmunoResearch) and developed by ECL 2 chemiluminescence (Pierce).

Fluo-3 AM staining and flow cytometry

Single cell suspensions were washed in PBS followed by staining with 2.5 uM Fluo-3 AM (Sigma) in FACS buffer (5% FBS in HBSS) and allowed to incubate for 20 mins on ice. 4 volumes of FACS buffer were then added and samples were incubated for an additional 40 mins at 37º C without CO_2. After washing, samples were acquired on the Canto-II (BD Bioscience). Raw data were analyzed with FlowJo v10.

LentiCRISPR targeting

VSV-G pseudotyped, self-inactivating lentivirus was prepared by transfecting a 60-80% confluent 10-cm plate of HEK 293T cells with 1.5 µg of pVSV-G expression vector, 3 µg of pMDLg/pRRE, 3 µg pRSV-Rev and 6 µg of pRRL lentiCRISPR vectors using Poly(ethyleneimine) (PEI; Sigma). Media was replaced 24 hours post-transfection and harvested 24 hours later for filtration with a 0.45 µm filter (SteriFlip, Millipore). Approximately 1 million cells were transduced with 10 mL filtered virus. Following 3-5 days of selection in appropriate antibiotic, successful targeting was verified through population-level Sanger sequencing and analysis using Tracking of Indels by DEcomposition (TIDE)[90].

For CRISPR/Cas9 gene targeting, we generated pRRL lentiviral vectors in which a U6 promoter drives expression of a gRNA, and an MND promoter drives expression of Cas9, a T2A peptide, and either puromycin or hygromycin resistance[49]. Primary mouse cells targeted in Fig. 3 received lentivirus that did not encode Cas9, as the cells came from mice that have constitutive Cas9 expression. gRNA sequences were designed using Benchling. gRNA sequences are as follows, where the (G) denotes a nucleotide added to enable robust transcription off the U6 promoter and the underlined sequence denotes the Protospacer Adjacent Motif (PAM):

Murine M1 non-targeting control: GCGAGGTATTCGGCTCCGCG[90]

Murine *Abcc1* guide 1: (G)TCAGAACACGGTCCTCACAT

Murine *Abcc1* guide 2: (G)TGGGCTGACCAGTAACACTG

Murine *Abcc3:* (G)ACACCACAGCAGAACACCGA

Murine *Abcc4:* (G)TGCGAGCCAAGAAGGACTCG

Murine *Abcc5:* (G)TCCGGAACCTGGGTTCCTCG

Murine *Abcc6:* (G)TGAAGAGGTGGGACATCCGG

Murine *Abcc10:* (G)TACTAGGCACCGACTCCGAG

Human H1 non-targeting control: (G)ACGGAGGCTAAGCGTCGCAA[90]

Human *ABCC1* guide 1: (G)ATAGACAGCCCCAATGACAG

Human *ABCC1* guide 2: (G)ACGATGATGACGTCCACCTG

Cloning and of ABCC1

PCR and In-Fusion cloning (Takara Clontech) were used to generate ABCC1 constructs. WT and K1333M mutant human ABCC1 constructs were generated using a human ABCC1 cDNA clone (Transomic, Clone ID TOH6003) as template. Mouse WT and K13330 mutant ABCC1 constructs were generated using a mouse ABCC1 cDNA clone (Transomic, Clone ID BC090617) as template.

Vesicle Transport Assays

We used inside-out plasma membrane vesicles derived from Sf9 cells (SBVT04 for hMRP1 and SBCT03 for control; Sigma Aldrich) to determine whether cGAMP is a direct substrate of ABCC1/MRP1. All reagents were prepared in incubation buffer (10 mM Tris-HCl, 10 mM MgCl2, 250 mM sucrose, pH 7.0) and incubated for 3 minutes at 37º C prior to use in the reactions. Reactions were initiated by adding ATP or AMP (for a final concentration of 5 mM) to 50 µg vesicles with or without 2'3' cGAMP (final concentration 5 µM). Some reactions also contained 1 mM glutathione (GSH). Reactions were incubated in 96-well plates for 2.5, 5, 10, or 20 minutes at 37º C. Reactions were terminated by putting plates on ice and adding 200 µl pre-chilled wash buffer per well (10 mM Tris-HCl, 100 mM NaCl, 250 mM sucrose) and transferred to a prewet 96-well filtration plate (EMD Millipore; MSFBN6B10). Each well was washed 5 times with 200 µl wash buffer under vacuum pressure. The trapped vesicles were lysed by addition of 100 µl RIPA lysis buffer and eluted into collection plates. Samples were subsequently assayed for cGAMP by ELISA, (Arbor Assays; K067). We used three distinct lots of ABCC1 vesicles and two distinct lots of control vesicles with similar results.

Quantitative RT-PCR

For quantitative RT-PCR analysis, triplicate cell samples or 50 uL fresh mouse blood were harvested into Trizol reagent before purification via Direct-zol RNA miniprep (Zymo Research) per manufacturer's instructions with an additional dry spin after disposing of the final wash to prevent carryover. cDNA was generated using EcoDry premix (Takara Bio). Samples were assayed in duplicate and transcript expression was measured using iTaq Universal SYBR green supermix (BioRad) on the Bio-Rad CFX96 Real-Time system.

Human gene PCR primer sequences are as follows:

GAPDH Fwd: 5'-AACAGCCTCAAGATCATCAGC-3', *GAPDH* Rev: 5'-CACCACCTTCTTGATGTCATC-3',

IFNB1 Fwd: 5'-ACGCCGCATTGACCATCTATG-3', *IFNB1* Rev: 5'-CGGAGGTAACCTGTAAGTCTGT-3'.

Mouse gene PCR primer sequences are as follows:

Hprt Fwd: 5'-GTTGGATACAGGCCAGATTTGTTG-3', *Hprt* Rev: 5'-GAGGGTAGGCTGGCCTATAGGCT-3',

Abcc1 Fwd: 5'-CTCTATCTCTCCCGACATGACC-3', *Abcc1* Rev: 5'-AGCAGACGATCCACAGCAAAA-3',

Abcc2 Fwd: 5'-CCCTGCTGTTCGATATACCAATC-3', *Abcc2* Rev: 5'-TCGAGAGAATCCAGAATAGGGAC-3',

Abcc3 Fwd: 5'-CTGTGCACACAGAAAACCCG-3', *Abcc3* Rev: 5'-GGACACCCAGGACCATCTTG-3',

Abcc4 Fwd: 5'-AGCTGAGAATGACGCACAGAA-3', *Abcc4* Rev: 5'-ATATGGGCTGGATTACTTTGGC-3',

Abcc5 Fwd: 5’-AGTCCTGGGTATAGAAGTGTGAG-3', *Abcc5* Rev: 5’-ATTCCAACGGTCGAGTTCTCC-3',

Abcc6 Fwd: 5’-AAGGAGGTACTAGGTGGGCTT-3', *Abcc6* Rev: 5’-CCAGTAGGACCCTTCGAGC-3',

Abcc10 Fwd: 5’-CCTAGTGCTGACCGTGTTGT-3', *Abcc10* Rev: 5’-TAGGTTGGCTGCAGTCTGTG-3',

Abcc12 Fwd: 5’-ATGATGCCGGGCTACTCTC-3', *Abcc12* Rev: 5’-CAGGGTGTCTACGGTCAGC-3',

Ifnb Fwd: 5’-GCACTGGGTGGAATGAGACTATTG-3’ *Ifnb* Rev: 5’-TTCTGAGGCATCAACTGACAGGTC -3’,

Cxcl10 Fwd: 5’-AAGTGCTGCCGTCATTTTCTGCCTC-3', *Cxcl10* Rev: 5’-CTTGATGGTCTTAGATTCCGGATTC-3',

Mx1 Fwd: 5’-GACCATAGGGGTCTTGACCAA-3', *Mx1* Rev: 5’-AGACTTGCTCTTTCTGAAAAGCC-3',

Isg15 Fwd: 5’-GGTGTCCGTGACTAACTCCAT-3', *Isg15* Rev: 5’-TGGAAAGGGTAAGACCGTCCT-3'.

HSV-1 Infections

WT-HSV-1 strain KOS were prepared in Vero cells, using a multiplicity of infection (MOI) of 0.01 for 48 hours before virus-containing medium was collected, spun down to remove any cells, and aliquoted for storage at -80º C. Titering was performed by serial dilution and plaque assay on the appropriate Vero cell line. Plaques were visualized by fixing/staining in 20% methanol with 0.2% crystal violet.

CXCL10 ELISA

Mouse blood was collected into Eppendorf tubes and allowed to clot for 45 minutes at room temperature, followed by two rounds of centrifugation and collection of top serum layer. Serum samples were assayed directly with Mouse IP-10 (CXCL10) ELISA Kit (Abcam) and analyzed per manufacturer's instructions.

Histology and Pathology

Tissues were fixed in 10% neutral buffered formalin and routinely paraffin embedded. Tissue sections (5μm) were stained with hematoxylin and eosin and histological scores were assigned in a blinded manner as previously described[83] with the following modifications: histology scores for skin and subcutaneous muscles of the head were combined; scores for the kidney reflect both inflammation scores for the interstitium as well as the extent of pathology. Images were captured from glass slides using NIS-Elements BR 3.2 64-bit and plated in Adobe Photoshop Elements. Image white balance, lighting, and contrast were adjusted using auto corrections applied to the entire image. Original magnification is stated.

Experimental replicates and statistics

Quantitative data were visualized and analyzed using GraphPad Prism software, ImageJ, and FlowJo. Specific statistical tests and experimental replicate numbers are noted in the figure legends.

References

1. Janeway, C.A. (1989). Approaching the asymptote? Evolution and revolution in immunology. Cold Spring Harb Symp Quant Biol 54 Pt 1, 1-13.

2. Abedon, S.T. (2012). Bacterial 'immunity' against bacteriophages. Bacteriophage 2, 50-54.

3. Fire, A., Xu, S., Montgomery, M.K., Kostas, S.A., Driver, S.E. and Mello, C.C. (1998). Potent and specific genetic interference by double-stranded RNA in Caenorhabditis elegans. Nature 391, 806-811.

4. McNab, F., Mayer-Barber, K., Sher, A., Wack, A. and O'Garra, A. (2015). Type I interferons in infectious disease. Nat Rev Immunol 15, 87-103.

5. Iwasaki, A. and Medzhitov, R. (2004). Toll-like receptor control of the adaptive immune responses. Nat Immunol 5, 987-995.

6. Yamamoto, M., Sato, S., Hemmi, H., Hoshino, K., Kaisho, T., Sanjo, H., Takeuchi, O., Sugiyama, M., Okabe, M., Takeda, K. and Akira, S. (2003). Role of adaptor TRIF in the MyD88-independent toll-like receptor signaling pathway. Science 301, 640-643.

7. Honda, K., Yanai, H., Negishi, H., Asagiri, M., Sato, M., Mizutani, T., Shimada, N., Ohba, Y., Takaoka, A., Yoshida, N. and Taniguchi, T. (2005). IRF-7 is the master regulator of type-I interferon-dependent immune responses. Nature 434, 772-777.

8. Kato, H., Takeuchi, O., Sato, S., Yoneyama, M., Yamamoto, M., Matsui, K., Uematsu, S., Jung, A., Kawai, T., Ishii, K.J., Yamaguchi, O., Otsu, K., Tsujimura, T., Koh, C.S., Reis e Sousa, C., Matsuura, Y., Fujita, T. and Akira, S. (2006). Differential roles of MDA5 and RIG-I helicases in the recognition of RNA viruses. Nature 441, 101-105.

9. Sun, L., Wu, J., Du, F., Chen, X. and Chen, Z.J. (2013). Cyclic GMP-AMP synthase is a cytosolic DNA sensor that activates the type I interferon pathway. Science 339, 786-791.

10. Volkman, H.E., Cambier, S., Gray, E.E. and Stetson, D.B. (2019). Tight nuclear tethering of cGAS is essential for preventing autoreactivity. Elife 8.

11. Cao, D., Han, X., Fan, X., Xu, R.M. and Zhang, X. (2020). Structural basis for nucleosome-mediated inhibition of cGAS activity. Cell Res 30, 1088-1097.

12. Boyer, J.A., Spangler, C.J., Strauss, J.D., Cesmat, A.P., Liu, P., McGinty, R.K. and Zhang, Q. (2020). Structural basis of nucleosome-dependent cGAS inhibition. Science 370, 450-454.

13. Pathare, G.R., Decout, A., Glück, S., Cavadini, S., Makasheva, K., Hovius, R., Kempf, G., Weiss, J., Kozicka, Z., Guey, B., Melenec, P., Fierz, B., Thomä, N.H. and Ablasser, A. (2020). Structural mechanism of cGAS inhibition by the nucleosome. Nature 587, 668-672.

14. Zhao, B., Xu, P., Rowlett, C.M., Jing, T., Shinde, O., Lei, Y., West, A.P., Liu, W.R. and Li, P. (2020). The molecular basis of tight nuclear tethering and inactivation of cGAS. Nature 587, 673-677.

15. Michalski, S., de Oliveira Mann, C.C., Stafford, C.A., Witte, G., Bartho, J., Lammens, K., Hornung, V. and Hopfner, K.P. (2020). Structural basis for sequestration and autoinhibition of cGAS by chromatin. Nature 587, 678-682.

16. Ablasser, A., Goldeck, M., Cavlar, T., Deimling, T., Witte, G., Röhl, I., Hopfner, K.P., Ludwig, J. and Hornung, V. (2013). cGAS produces a 2'-5'-linked cyclic dinucleotide second messenger that activates STING. Nature 498, 380-384.

17. Gao, P., Ascano, M., Wu, Y., Barchet, W., Gaffney, B.L., Zillinger, T., Serganov, A.A., Liu, Y., Jones, R.A., Hartmann, G., Tuschl, T. and Patel, D.J. (2013). Cyclic [G(2',5')pA(3',5')p] is the

metazoan second messenger produced by DNA-activated cyclic GMP-AMP synthase. Cell 153, 1094-1107.

18. Barber, G.N. (2014). STING-dependent cytosolic DNA sensing pathways. Trends Immunol 35, 88-93.

19. Seth, R.B., Sun, L., Ea, C.K. and Chen, Z.J. (2005). Identification and characterization of MAVS, a mitochondrial antiviral signaling protein that activates NF-kappaB and IRF 3. Cell 122, 669-682.

20. Crowl, J.T., Gray, E.E., Pestal, K., Volkman, H.E. and Stetson, D.B. (2017). Intracellular Nucleic Acid Detection in Autoimmunity. Annu Rev Immunol 35, 313-336.

21. Crow, Y.J. and Manel, N. (2015). Aicardi-Goutières syndrome and the type I interferonopathies. Nat Rev Immunol 15, 429-440.

22. Stetson, D.B., Ko, J.S., Heidmann, T. and Medzhitov, R. (2008). Trex1 prevents cell-intrinsic initiation of autoimmunity. Cell 134, 587-598.

23. Reijns, M.A., Bubeck, D., Gibson, L.C., Graham, S.C., Baillie, G.S., Jones, E.Y. and Jackson, A.P. (2011). The structure of the human RNase H2 complex defines key interaction interfaces relevant to enzyme function and human disease. J Biol Chem 286, 10530-10539.

24. Kretschmer, S., Wolf, C., König, N., Staroske, W., Guck, J., Häusler, M., Luksch, H., Nguyen, L.A., Kim, B., Alexopoulou, D., Dahl, A., Rapp, A., Cardoso, M.C., Shevchenko, A. and Lee-Kirsch, M.A. (2015). SAMHD1 prevents autoimmunity by maintaining genome stability. Ann Rheum Dis 74, e17.

25. Eckard, S.C., Rice, G.I., Fabre, A., Badens, C., Gray, E.E., Hartley, J.L., Crow, Y.J. and Stetson, D.B. (2014). The SKIV2L RNA exosome limits activation of the RIG-I-like receptors. Nat Immunol 15, 839-845.

26. Liddicoat, B.J., Piskol, R., Chalk, A.M., Ramaswami, G., Higuchi, M., Hartner, J.C., Li, J.B., Seeburg, P.H. and Walkley, C.R. (2015). RNA editing by ADAR1 prevents MDA5 sensing of endogenous dsRNA as nonself. Science 349, 1115-1120.

27. Woodward, J.J., Iavarone, A.T. and Portnoy, D.A. (2010). c-di-AMP secreted by intracellular Listeria monocytogenes activates a host type I interferon response. Science 328, 1703-1705.

28. Kranzusch, P.J., Wilson, S.C., Lee, A.S., Berger, J.M., Doudna, J.A. and Vance, R.E. (2015). Ancient Origin of cGAS-STING Reveals Mechanism of Universal 2',3' cGAMP Signaling. Mol Cell 59, 891-903.

29. Nelson, J.W. and Breaker, R.R. (2017). The lost language of the RNA World. Sci Signal 10.

30. Li, L., Yin, Q., Kuss, P., Maliga, Z., Millán, J.L., Wu, H. and Mitchison, T.J. (2014). Hydrolysis of 2'3'-cGAMP by ENPP1 and design of nonhydrolyzable analogs. Nat Chem Biol 10, 1043-1048.

31. Ablasser, A., Schmid-Burgk, J.L., Hemmerling, I., Horvath, G.L., Schmidt, T., Latz, E. and Hornung, V. (2013). Cell intrinsic immunity spreads to bystander cells via the intercellular transfer of cGAMP. Nature 503, 530-534.

32. Bridgeman, A., Maelfait, J., Davenne, T., Partridge, T., Peng, Y., Mayer, A., Dong, T., Kaever, V., Borrow, P. and Rehwinkel, J. (2015). Viruses transfer the antiviral second messenger cGAMP between cells. Science 349, 1228-1232.

33. Gentili, M., Kowal, J., Tkach, M., Satoh, T., Lahaye, X., Conrad, C., Boyron, M., Lombard, B., Durand, S., Kroemer, G., Loew, D., Dalod, M., Théry, C. and Manel, N. (2015). Transmission of innate immune signaling by packaging of cGAMP in viral particles. Science 349, 1232-1236.

34. Marcus, A., Mao, A.J., Lensink-Vasan, M., Wang, L., Vance, R.E. and Raulet, D.H. (2018). Tumor-Derived cGAMP Triggers a STING-Mediated Interferon Response in Non-tumor Cells to Activate the NK Cell Response. Immunity 49, 754-763.e754.

35. Carozza, J., Bohnert, V., Nguyen, K., Skariah, G., Shaw, K., Brown, J., Rafat, M., Eyben, R.v., Graves, E., Glenn, J., Smith, M. and Li, L. (2020). Extracellular cGAMP is a cancer-cell-produced immunotransmitter involved in radiation-induced anticancer immunity. Nature Cancer 1, 184-196.

36. Luteijn, R.D., Zaver, S.A., Gowen, B.G., Wyman, S.K., Garelis, N.E., Onia, L., McWhirter, S.M., Katibah, G.E., Corn, J.E., Woodward, J.J. and Raulet, D.H. (2019). SLC19A1 transports immunoreactive cyclic dinucleotides. Nature 573, 434-438.

37. Ritchie, C., Cordova, A.F., Hess, G.T., Bassik, M.C. and Li, L. (2019). SLC19A1 Is an Importer of the Immunotransmitter cGAMP. Mol Cell 75, 372-381.e375.

38. Lahey, L.J., Mardjuki, R.E., Wen, X., Hess, G.T., Ritchie, C., Carozza, J.A., Böhnert, V., Maduke, M., Bassik, M.C. and Li, L. (2020). LRRC8A:C/E Heteromeric Channels Are Ubiquitous Transporters of cGAMP. Mol Cell 80, 578-591.e575.

39. Zhou, C., Chen, X., Planells-Cases, R., Chu, J., Wang, L., Cao, L., Li, Z., López-Cayuqueo, K.I., Xie, Y., Ye, S., Wang, X., Ullrich, F., Ma, S., Fang, Y., Zhang, X., Qian, Z., Liang, X., Cai, S.Q., Jiang, Z., Zhou, D., Leng, Q., Xiao, T.S., Lan, K., Yang, J., Li, H., Peng, C., Qiu, Z., Jentsch, T.J. and Xiao, H. (2020). Transfer of cGAMP into Bystander Cells via LRRC8 Volume-

Regulated Anion Channels Augments STING-Mediated Interferon Responses and Anti-viral Immunity. Immunity 52, 767-781.e766.

40. Cordova, A.F., Ritchie, C., Böhnert, V. and Li, L. (2021). Human SLC46A2 Is the Dominant cGAMP Importer in Extracellular cGAMP-Sensing Macrophages and Monocytes. ACS Cent Sci 7, 1073-1088.

41. Zhou, Y., Fei, M., Zhang, G., Liang, W.C., Lin, W., Wu, Y., Piskol, R., Ridgway, J., McNamara, E., Huang, H., Zhang, J., Oh, J., Patel, J.M., Jakubiak, D., Lau, J., Blackwood, B., Bravo, D.D., Shi, Y., Wang, J., Hu, H.M., Lee, W.P., Jesudason, R., Sangaraju, D., Modrusan, Z., Anderson, K.R., Warming, S., Roose-Girma, M. and Yan, M. (2020). Blockade of the Phagocytic Receptor MerTK on Tumor-Associated Macrophages Enhances P2X7R-Dependent STING Activation by Tumor-Derived cGAMP. Immunity 52, 357-373.e359.

42. Dean, M., Rzhetsky, A. and Allikmets, R. (2001). The human ATP-binding cassette (ABC) transporter superfamily. Genome Res 11, 1156-1166.

43. Vasiliou, V., Vasiliou, K. and Nebert, D.W. (2009). Human ATP-binding cassette (ABC) transporter family. Hum Genomics 3, 281-290.

44. Robey, R.W., Pluchino, K.M., Hall, M.D., Fojo, A.T., Bates, S.E. and Gottesman, M.M. (2018). Revisiting the role of ABC transporters in multidrug-resistant cancer. Nat Rev Cancer 18, 452-464.

45. Sun, Y.L., Patel, A., Kumar, P. and Chen, Z.S. (2012). Role of ABC transporters in cancer chemotherapy. Chin J Cancer 31, 51-57.

46. Hornung, V., Ablasser, A., Charrel-Dennis, M., Bauernfeind, F., Horvath, G., Caffrey, D.R., Latz, E. and Fitzgerald, K.A. (2009). AIM2 recognizes cytosolic dsDNA and forms a caspase-1-activating inflammasome with ASC. Nature 458, 514-518.

47. Fink, S.L. and Cookson, B.T. (2005). Apoptosis, pyroptosis, and necrosis: mechanistic description of dead and dying eukaryotic cells. Infect Immun 73, 1907-1916.

48. Maelfait, J., Liverpool, L. and Rehwinkel, J. (2020). Nucleic Acid Sensors and Programmed Cell Death. J Mol Biol 432, 552-568.

49. Gray, E.E., Winship, D., Snyder, J.M., Child, S.J., Geballe, A.P. and Stetson, D.B. (2016). The AIM2-like Receptors Are Dispensable for the Interferon Response to Intracellular DNA. Immunity 45, 255-266.

50. Burleigh, K., Maltbaek, J.H., Cambier, S., Green, R., Gale, M., James, R.C. and Stetson, D.B. (2020). Human DNA-PK activates a STING-independent DNA sensing pathway. Sci Immunol 5.

51. Giard, D.J., Aaronson, S.A., Todaro, G.J., Arnstein, P., Kersey, J.H., Dosik, H. and Parks, W.P. (1973). In vitro cultivation of human tumors: establishment of cell lines derived from a series of solid tumors. J Natl Cancer Inst 51, 1417-1423.

52. Gey, G.O., Coffman, W.D. and Kubicek, M.T. (1952). Tissue culture studies of the proliferative capacity of cervical carcinoma and normal epithelium. Cancer Research 12, 264-265.

53. Valmori, D., Fonteneau, J.F., Lizana, C.M., Gervois, N., Liénard, D., Rimoldi, D., Jongeneel, V., Jotereau, F., Cerottini, J.C. and Romero, P. (1998). Enhanced generation of specific tumor-

reactive CTL in vitro by selected Melan-A/MART-1 immunodominant peptide analogues. J Immunol 160, 1750-1758.

54. Safa, A.R. (1988). Photoaffinity labeling of the multidrug-resistance-related P-glycoprotein with photoactive analogs of verapamil. Proc Natl Acad Sci U S A 85, 7187-7191.

55. Allen, J.D., van Loevezijn, A., Lakhai, J.M., van der Valk, M., van Tellingen, O., Reid, G., Schellens, J.H., Koomen, G.J. and Schinkel, A.H. (2002). Potent and specific inhibition of the breast cancer resistance protein multidrug transporter in vitro and in mouse intestine by a novel analogue of fumitremorgin C. Mol Cancer Ther 1, 417-425.

56. Dean, M. and Annilo, T. (2005). Evolution of the ATP-binding cassette (ABC) transporter superfamily in vertebrates. Annu Rev Genomics Hum Genet 6, 123-142.

57. Weidner, L.D., Zoghbi, S.S., Lu, S., Shukla, S., Ambudkar, S.V., Pike, V.W., Mulder, J., Gottesman, M.M., Innis, R.B. and Hall, M.D. (2015). The Inhibitor Ko143 Is Not Specific for ABCG2. J Pharmacol Exp Ther 354, 384-393.

58. Leier, I., Jedlitschky, G., Buchholz, U., Cole, S.P., Deeley, R.G. and Keppler, D. (1994). The MRP gene encodes an ATP-dependent export pump for leukotriene C4 and structurally related conjugates. J Biol Chem 269, 27807-27810.

59. Cole, S.P. (2014). Multidrug resistance protein 1 (MRP1, ABCC1), a "multitasking" ATP-binding cassette (ABC) transporter. J Biol Chem 289, 30880-30888.

60. Mitra, P., Oskeritzian, C.A., Payne, S.G., Beaven, M.A., Milstien, S. and Spiegel, S. (2006). Role of ABCC1 in export of sphingosine-1-phosphate from mast cells. Proc Natl Acad Sci U S A 103, 16394-16399.

61. Reid, G., Wielinga, P., Zelcer, N., De Haas, M., Van Deemter, L., Wijnholds, J., Balzarini, J. and Borst, P. (2003). Characterization of the transport of nucleoside analog drugs by the human multidrug resistance proteins MRP4 and MRP5. Mol Pharmacol 63, 1094-1103.

62. Barrington, R.D., Needs, P.W., Williamson, G. and Kroon, P.A. (2015). MK571 inhibits phase-2 conjugation of flavonols by Caco-2/TC7 cells, but does not specifically inhibit their apical efflux. Biochem Pharmacol 95, 193-200.

63. Platt, R.J., Chen, S., Zhou, Y., Yim, M.J., Swiech, L., Kempton, H.R., Dahlman, J.E., Parnas, O., Eisenhaure, T.M., Jovanovic, M., Graham, D.B., Jhunjhunwala, S., Heidenreich, M., Xavier, R.J., Langer, R., Anderson, D.G., Hacohen, N., Regev, A., Feng, G., Sharp, P.A. and Zhang, F. (2014). CRISPR-Cas9 knockin mice for genome editing and cancer modeling. Cell 159, 440-455.

64. Brunette, R.L., Young, J.M., Whitley, D.G., Brodsky, I.E., Malik, H.S. and Stetson, D.B. (2012). Extensive evolutionary and functional diversity among mammalian AIM2-like receptors. J Exp Med 209, 1969-1983.

65. Brinkman, E.K., Chen, T., Amendola, M. and van Steensel, B. (2014). Easy quantitative assessment of genome editing by sequence trace decomposition. Nucleic Acids Res 42, e168.

66. Keppler, D., Cui, Y., König, J., Leier, I. and Nies, A. (1999). Export pumps for anionic conjugates encoded by MRP genes. Adv Enzyme Regul 39, 237-246.

67. Prechtl, S., Roellinghoff, M., Scheper, R., Cole, S.P., Deeley, R.G. and Lohoff, M. (2000). The multidrug resistance protein 1: a functionally important activation marker for murine Th1 cells. J Immunol 164, 754-761.

68. Wielinga, P.R., van der Heijden, I., Reid, G., Beijnen, J.H., Wijnholds, J. and Borst, P. (2003). Characterization of the MRP4- and MRP5-mediated transport of cyclic nucleotides from intact cells. J Biol Chem 278, 17664-17671.

69. Jedlitschky, G., Burchell, B. and Keppler, D. (2000). The multidrug resistance protein 5 functions as an ATP-dependent export pump for cyclic nucleotides. J Biol Chem 275, 30069-30074.

70. Guo, Y., Kotova, E., Chen, Z.S., Lee, K., Hopper-Borge, E., Belinsky, M.G. and Kruh, G.D. (2003). MRP8, ATP-binding cassette C11 (ABCC11), is a cyclic nucleotide efflux pump and a resistance factor for fluoropyrimidines 2',3'-dideoxycytidine and 9'-(2'-phosphonylmethoxyethyl)adenine. J Biol Chem 278, 29509-29514.

71. Whiteley, A.T., Eaglesham, J.B., de Oliveira Mann, C.C., Morehouse, B.R., Lowey, B., Nieminen, E.A., Danilchanka, O., King, D.S., Lee, A.S.Y., Mekalanos, J.J. and Kranzusch, P.J. (2019). Bacterial cGAS-like enzymes synthesize diverse nucleotide signals. Nature 567, 194-199.

72. Lowey, B., Whiteley, A.T., Keszei, A.F.A., Morehouse, B.R., Mathews, I.T., Antine, S.P., Cabrera, V.J., Kashin, D., Niemann, P., Jain, M., Schwede, F., Mekalanos, J.J., Shao, S., Lee, A.S.Y. and Kranzusch, P.J. (2020). CBASS Immunity Uses CARF-Related Effectors to Sense 3'-5'- and 2'-5'-Linked Cyclic Oligonucleotide Signals and Protect Bacteria from Phage Infection. Cell 182, 38-49.e17.

73. Gui, X., Yang, H., Li, T., Tan, X., Shi, P., Li, M., Du, F. and Chen, Z.J. (2019). Autophagy induction via STING trafficking is a primordial function of the cGAS pathway. Nature 567, 262-266.

74. Morehouse, B.R., Govande, A.A., Millman, A., Keszei, A.F.A., Lowey, B., Ofir, G., Shao, S., Sorek, R. and Kranzusch, P.J. (2020). STING cyclic dinucleotide sensing originated in bacteria. Nature 586, 429-433.

75. Burroughs, A.M., Zhang, D., Schäffer, D.E., Iyer, L.M. and Aravind, L. (2015). Comparative genomic analyses reveal a vast, novel network of nucleotide-centric systems in biological conflicts, immunity and signaling. Nucleic Acids Res 43, 10633-10654.

76. Higgins, C.F. (1992). ABC transporters: from microorganisms to man. Annu Rev Cell Biol 8, 67-113.

77. Gao, M., Cui, H.R., Loe, D.W., Grant, C.E., Almquist, K.C., Cole, S.P. and Deeley, R.G. (2000). Comparison of the functional characteristics of the nucleotide binding domains of multidrug resistance protein 1. J Biol Chem 275, 13098-13108.

78. Steck, T.L., Weinstein, R.S., Straus, J.H. and Wallach, D.F. (1970). Inside-out red cell membrane vesicles: preparation and purification. Science 168, 255-257.

79. Johnson, Z.L. and Chen, J. (2017). Structural Basis of Substrate Recognition by the Multidrug Resistance Protein MRP1. Cell 168, 1075-1085.e1079.

80. Crow, Y.J., Hayward, B.E., Parmar, R., Robins, P., Leitch, A., Ali, M., Black, D.N., van Bokhoven, H., Brunner, H.G., Hamel, B.C., Corry, P.C., Cowan, F.M., Frints, S.G., Klepper, J., Livingston, J.H., Lynch, S.A., Massey, R.F., Meritet, J.F., Michaud, J.L., Ponsot, G., Voit, T., Lebon, P., Bonthron, D.T., Jackson, A.P., Barnes, D.E. and Lindahl, T. (2006). Mutations in the gene encoding the 3'-5' DNA exonuclease TREX1 cause Aicardi-Goutieres syndrome at the AGS1 locus. Nat Genet 38, 917-920.

81. Gray, E.E., Treuting, P.M., Woodward, J.J. and Stetson, D.B. (2015). Cutting Edge: cGAS Is Required for Lethal Autoimmune Disease in the Trex1-Deficient Mouse Model of Aicardi-Goutieres Syndrome. J Immunol 195, 1939-1943.

82. Gao, D., Li, T., Li, X.D., Chen, X., Li, Q.Z., Wight-Carter, M. and Chen, Z.J. (2015). Activation of cyclic GMP-AMP synthase by self-DNA causes autoimmune diseases. Proc Natl Acad Sci U S A 112, E5699-5705.

83. Gall, A., Treuting, P., Elkon, K.B., Loo, Y.M., Gale, M., Barber, G.N. and Stetson, D.B. (2012). Autoimmunity initiates in nonhematopoietic cells and progresses via lymphocytes in an interferon-dependent autoimmune disease. Immunity 36, 120-131.

84. Liu, S., Cai, X., Wu, J., Cong, Q., Chen, X., Li, T., Du, F., Ren, J., Wu, Y.T., Grishin, N.V. and Chen, Z.J. (2015). Phosphorylation of innate immune adaptor proteins MAVS, STING, and TRIF induces IRF3 activation. Science 347, aaa2630.

85. Lorico, A., Rappa, G., Finch, R.A., Yang, D., Flavell, R.A. and Sartorelli, A.C. (1997). Disruption of the murine MRP (multidrug resistance protein) gene leads to increased sensitivity to etoposide (VP-16) and increased levels of glutathione. Cancer Res 57, 5238-5242.

86. Li, L., Yin, Q., Kuss, P., Maliga, Z., Millan, J.L., Wu, H. and Mitchison, T.J. (2014). Hydrolysis of 2'3'-cGAMP by ENPP1 and design of nonhydrolyzable analogs. Nat Chem Biol 10, 1043-1048.

87. Gray, E.E., Treuting, P.M., Woodward, J.J. and Stetson, D.B. (2015). Cutting Edge: cGAS Is Required for Lethal Autoimmune Disease in the Trex1-Deficient Mouse Model of Aicardi-Goutières Syndrome. J Immunol 195, 1939-1943.

88. Orozco, S., Yatim, N., Werner, M.R., Tran, H., Gunja, S.Y., Tait, S.W., Albert, M.L., Green, D.R. and Oberst, A. (2014). RIPK1 both positively and negatively regulates RIPK3 oligomerization and necroptosis. Cell Death Differ 21, 1511-1521.

89. Saito, T., Owen, D.M., Jiang, F., Marcotrigiano, J. and Gale, M. (2008). Innate immunity induced by composition-dependent RIG-I recognition of hepatitis C virus RNA. Nature 454, 523-527.

90. Sanjana, N.E., Shalem, O. and Zhang, F. (2014). Improved vectors and genome-wide libraries for CRISPR screening. Nat Methods 11, 783-784.